Gravitational lensing in alternative gravity theories

László Árpád Gergely

University of Szeged, Hungary

with

Zsolt Horváth, Zoltán Keresztes, Marek Dwornik *(Szeged)*,
David Hobill *(Calgary)*,
Francisco F. S. Lobo *(Lisboa)*,
Salvatore Capozziello, Mariafelicia de Laurentis *(Napoli)*,
K.T. Wong, K.S. Cheng, Tiberiu Harko *(Hong Kong)*

based on:

Class. Quantum Grav. **26**, 145002-1-11 (2009)
Class. Quantum Grav. **27**, 235006-1-21 (2010)
Phys. Rev. D **84**, 083006-1-9 (2011)
Phys. Rev. D **86**, 044038-1-15 (2012)
arXiv:1203.6576 [gr-qc]
arXiv:1207.1823 [gr-qc]

2012

there is a fundamental issue:

Are extragalactic observations and cosmology probing the breakdown of General Relativity at large (IR) scales?

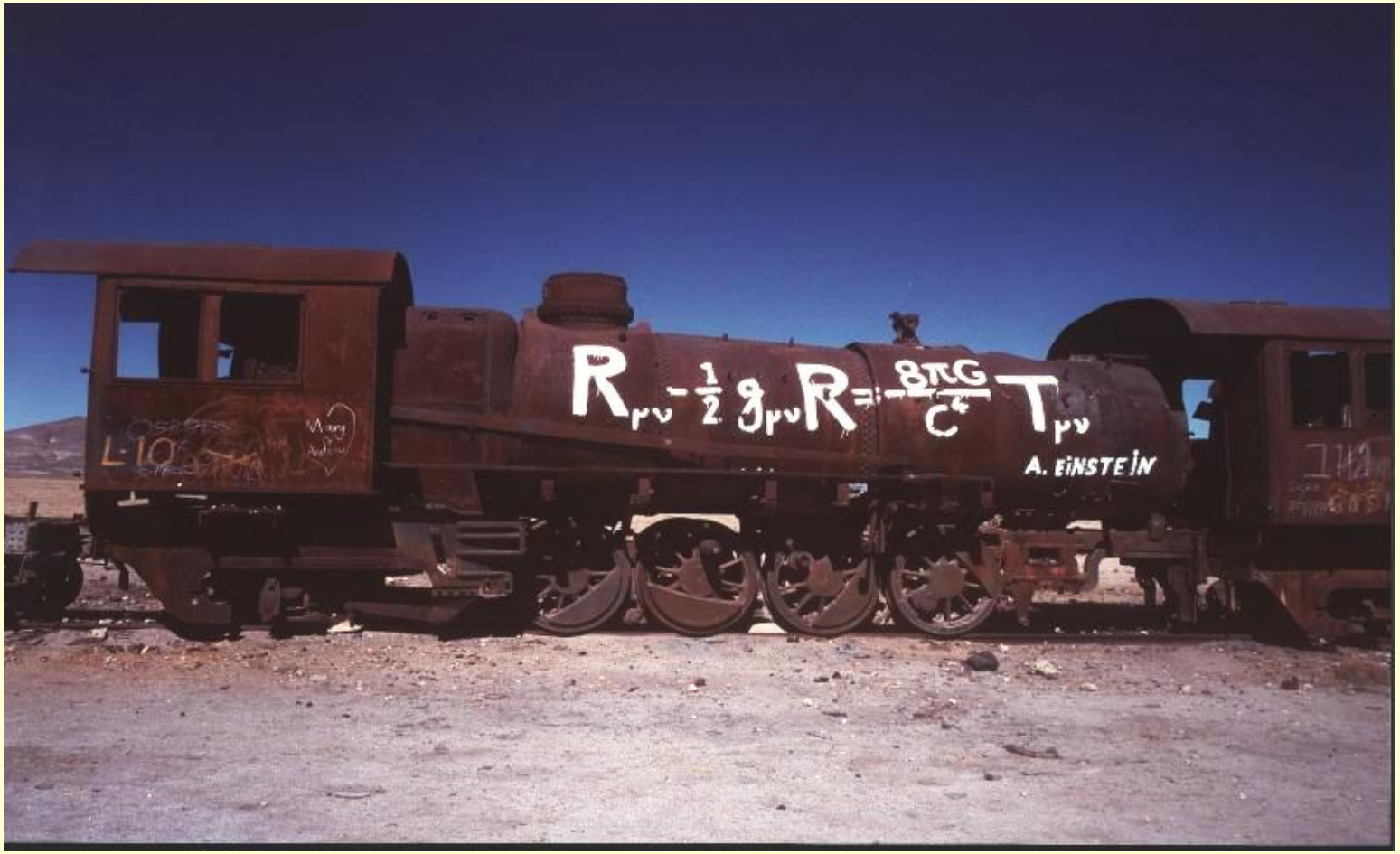

Slide courtesy of Salvatore Capozziello

Dark Energy and *w*
(the EoS viewpoint)

In GR, force $\propto (\rho + 3p)$

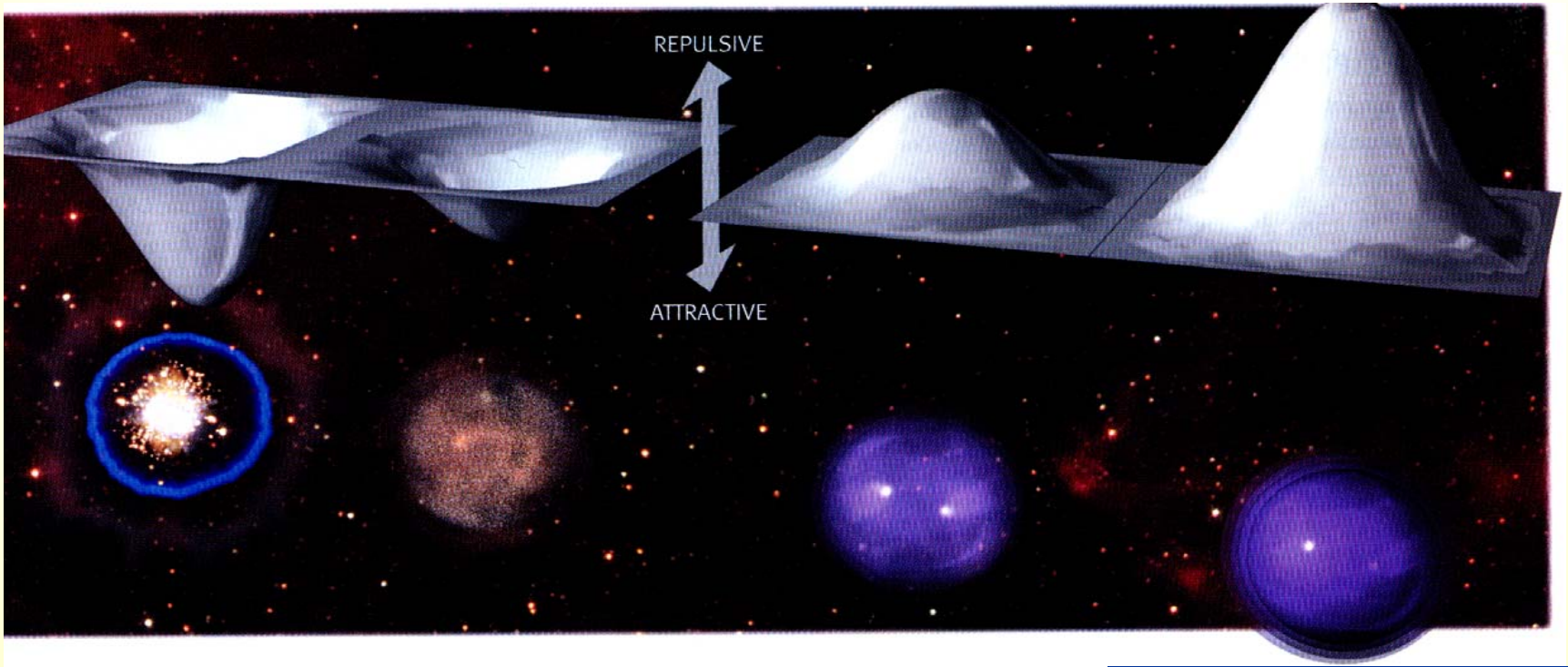

$w = p/\rho =$ +1/3 | 0 | -1 <*w*< -1/3 | -1

If *w* < -1/3 the Universe accelerates, *w* < -1, phantom fields

Slide courtesy of Salvatore Capozziello

The problem could be reversed

We are able to observe only baryons, radiation, neutrinos and gravity

Dark Energy and Dark Matter as "shortcomings" of GR.

Results of flawed physics?

The "correct" theory of gravity could be derived by matching the largest number of observations at ALL SCALES!

Accelerating behaviour (DE) and dynamical phenomena (DM) as ***CURVATURE EFFECTS***

Slide courtesy of Salvatore Capozziello

Two ways compete

- Einstein-equation:

$$G_{ab} = 8\pi G\, T_{ab}$$

- modified with dark matter, dark energy terms:

$$G_{ab} = 8\pi G\, \left(T + \text{unusual matter}\right)_{ab}$$

- modified gravitational dynamics

$$\left[G + f\left(\text{metric, extrinsic curvature}\right)\right]_{ab} = 8\pi G\, T_{ab}$$

Outline

Dark matter, dark energy, quantization → alternative gravity

Ways to test: weak and strong gravitational lensing (static case, spherical symmetry)

1. Tidal charged brane black hole
2. Dark radiation / pressure dominated brane-world models
3. Kehagias-Sfetsos black hole in Hořava-Lifsitz gravity
4. Black holes in fourth order f(R) gravity

Outline 2

Main results:

1. observational signatures between lensing observables
2. critical phenomena

Implications: constrain the extra BH parameters (beside mass), of alternative gravity origin

Deflection of light

Prediction: ***Light is curved by mass / energy (general relativity)***

Our Sun:

- deflection of light calculated as

$$\Delta\phi = \frac{4GM}{c^2 b}.$$

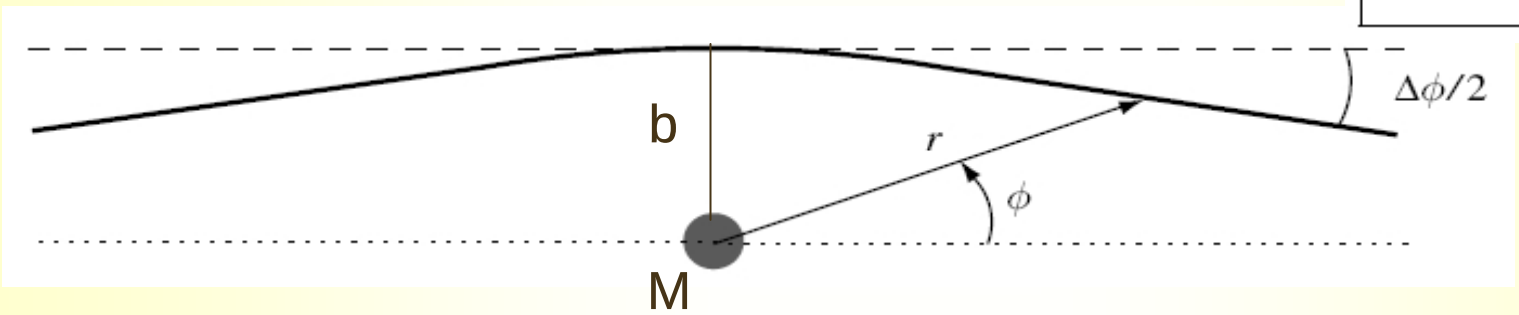

- numerically for the light ray passing near the Sun $\Delta\phi = 1''.75$

- Eddington 1919:

$$\Delta\phi = 1''.98 \pm 0''.16,$$
$$\Delta\phi = 1''.61 \pm 0''.4,$$

Gravitational lensing by BHs

Gravitational vs. optical lensing:

a) focal-axis
b) focal-point

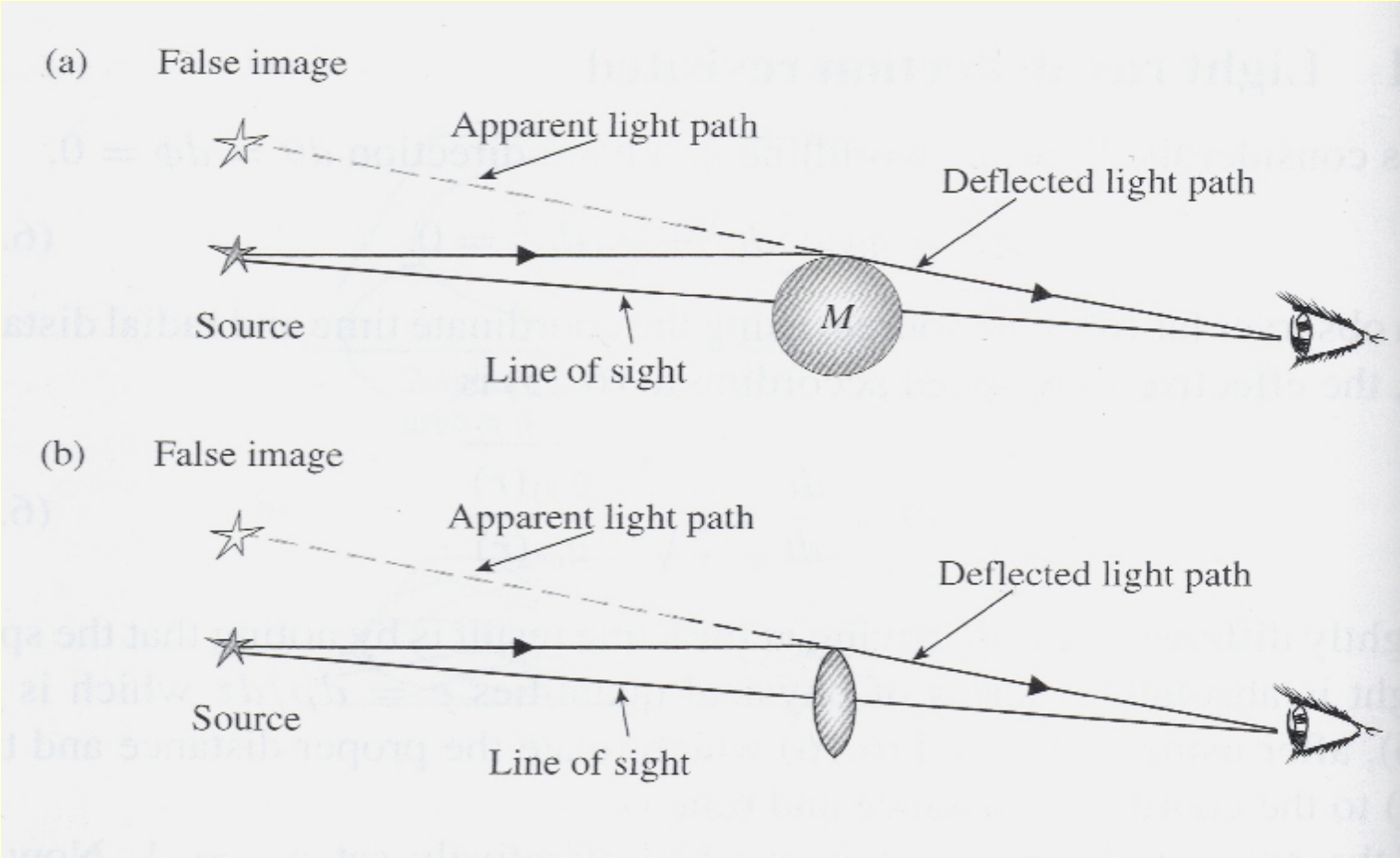

Cheng: *Relativity, Gravitation and Cosmology* (2005)

Gravitational lensing by BHs

Einstein-ring:

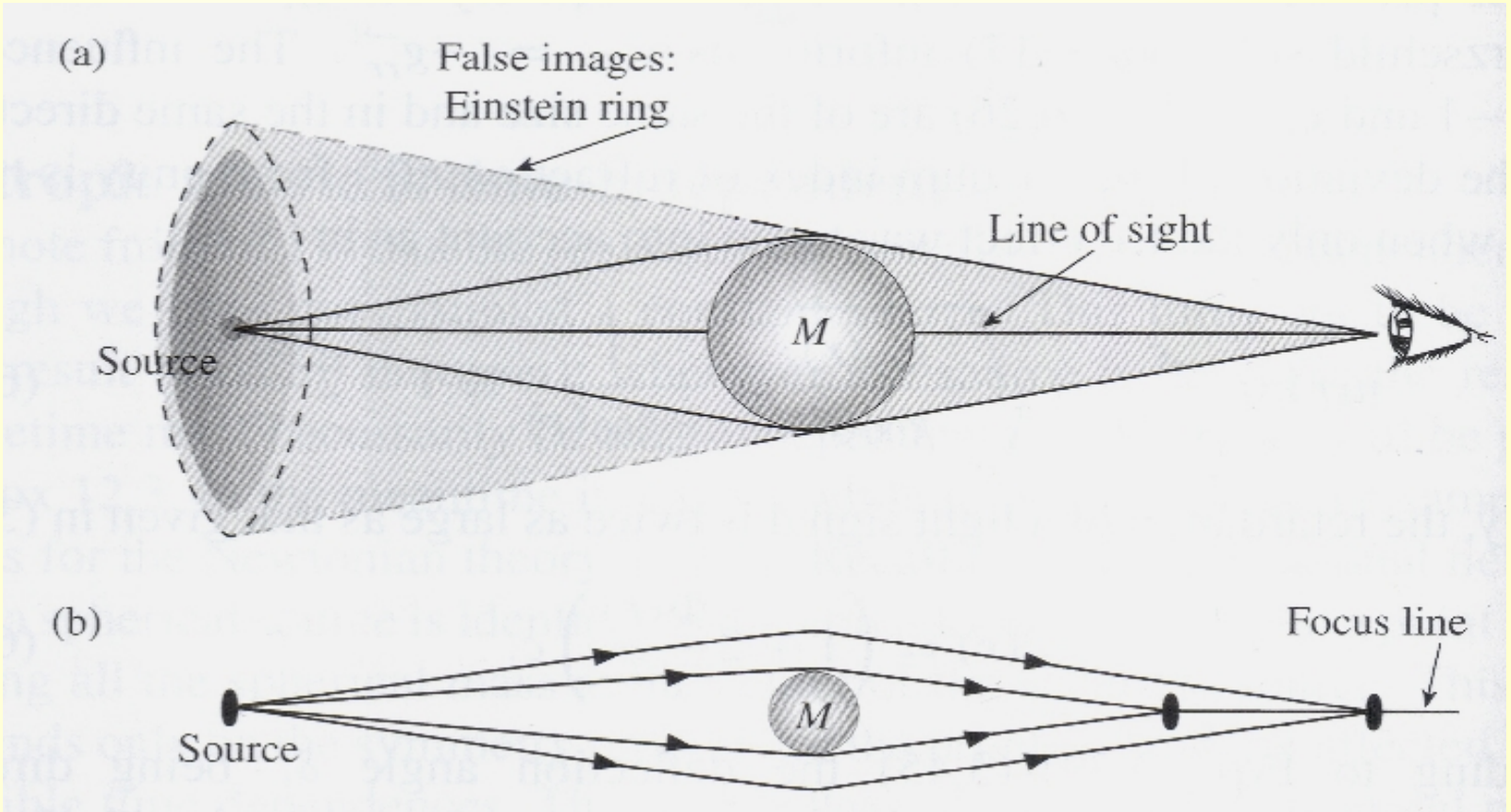

Cheng: *Relativity, Gravitation and Cosmology* (2005)

Gravitational lensing

Weak lensing: the images acquire shear

→Shear *statistics*: (dark) matter distribution in the Universe

Intermediate and strong lensing:

→ suitable in certain cases for determining distances

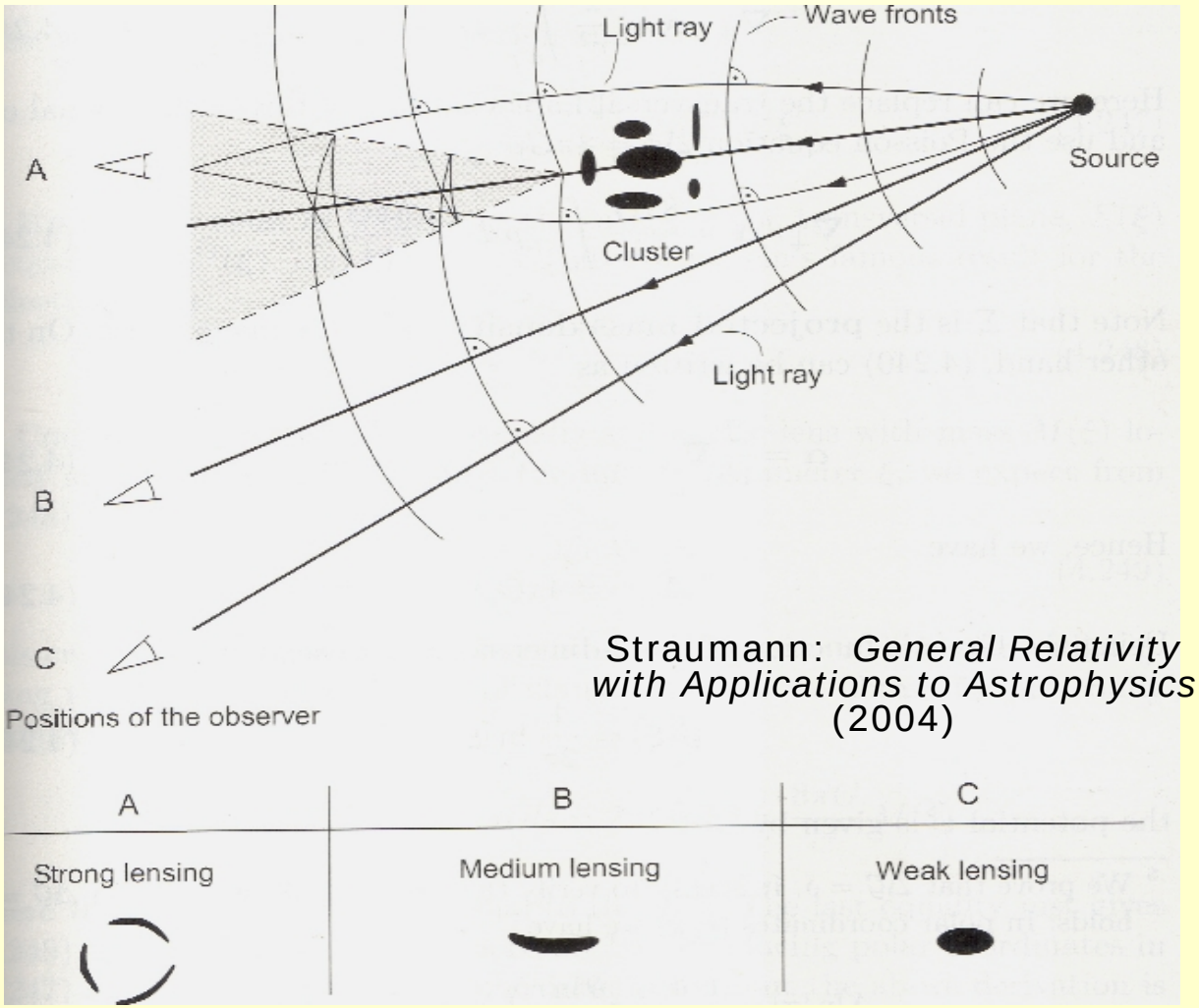

Straumann: *General Relativity with Applications to Astrophysics* (2004)

Abell 2218 galaxy cluster as a gravitational lens

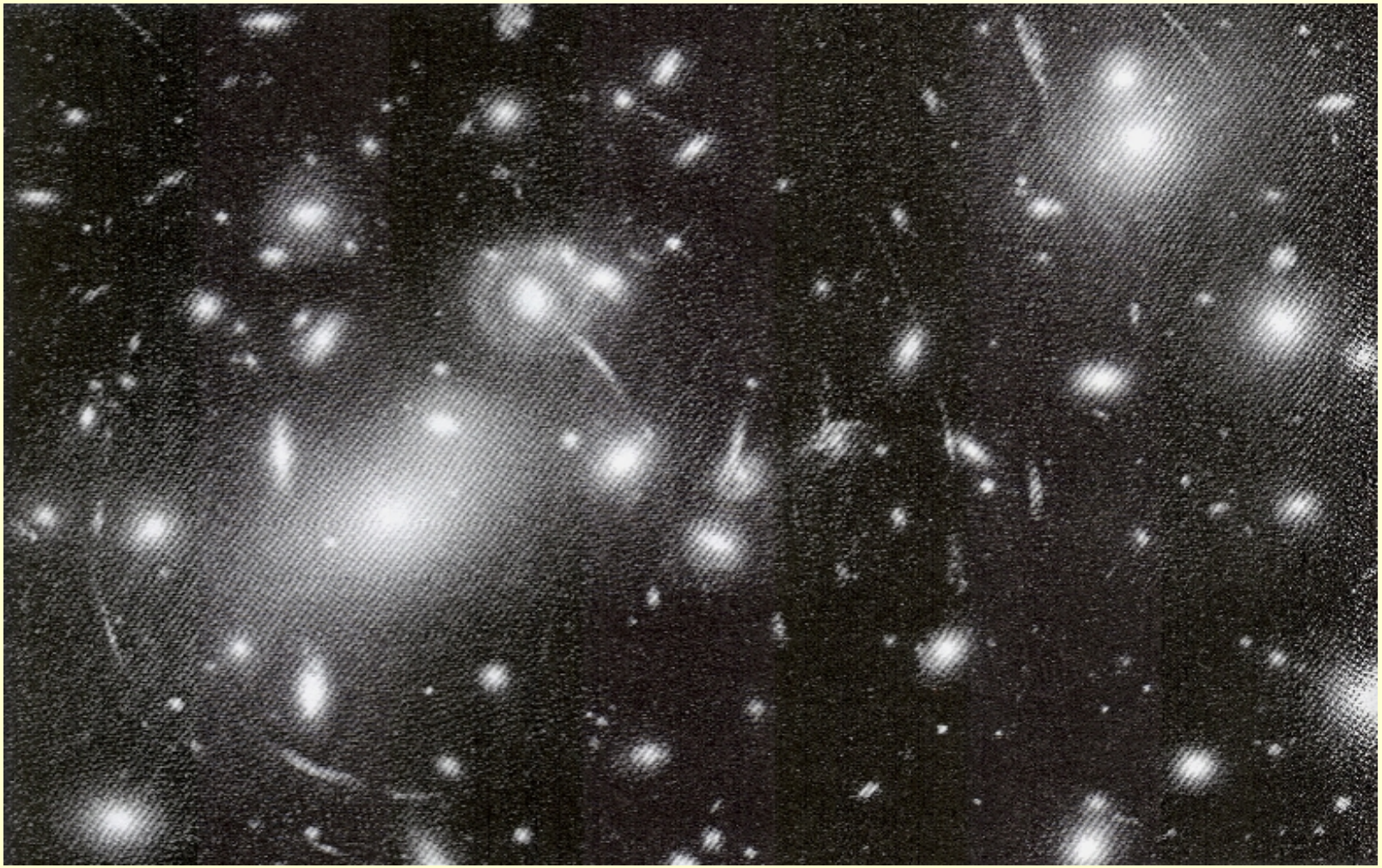

Hubble
Space
Telescope

Deflection angle in weak gravitational lensing

- first order contributions to deflection given by the Virbhadra-Ellis lens equation

$$0 = \tan|\theta| - \tan(s\beta) - \frac{D_{ls}}{D_s}\left[\tan|\theta| + \tan(\delta - |\theta|)\right] \ .$$

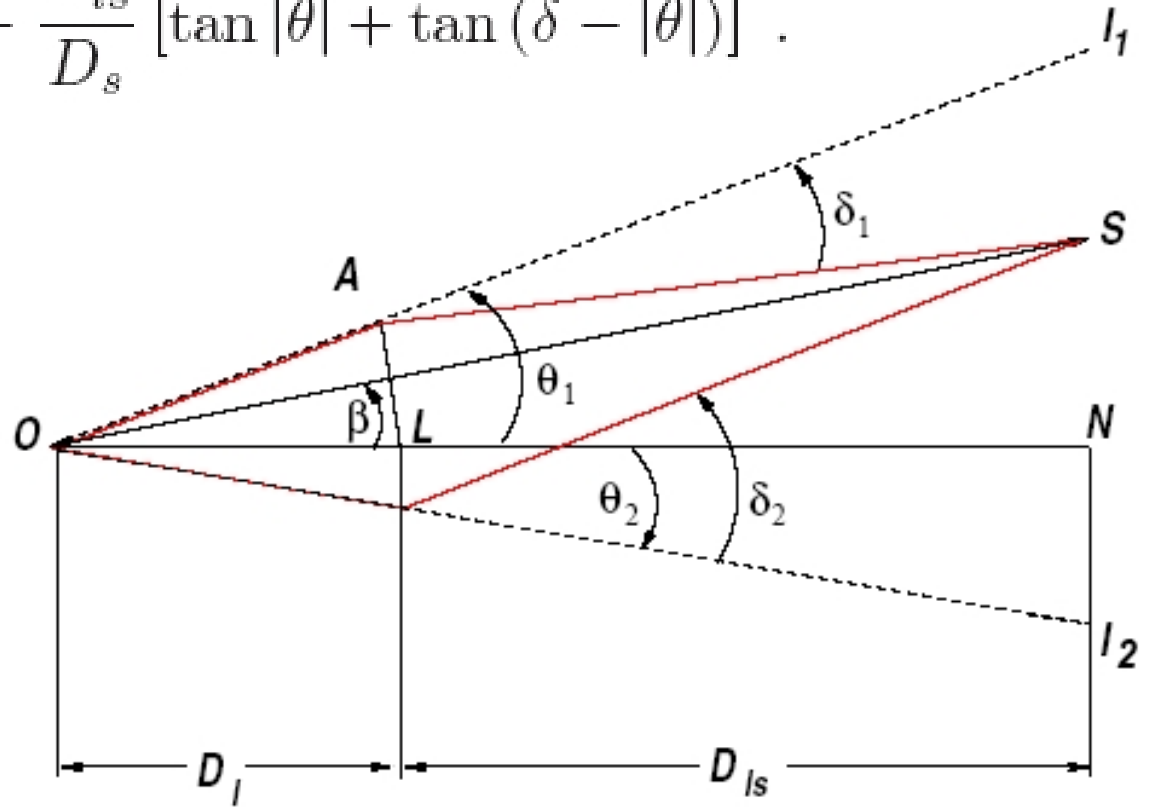

Image formation in weak gravitational lensing by tidal charged black holes

LÁ Gergely, Z Keresztes, M Dwornik

Class. Quantum Grav. 26, 145002 (2009) *[arXiv: 0903.1558 [gr-qc]]*

Z Horváth, LÁ Gergely, D Hobill

Class. Quantum Grav. 27, 235006 (2010) *[arXiv: 1005.2286 [gr-qc]]*

What is a brane? A hypersurface in a higher dimensional pseudo-Riemannian space-time (in 2d: membrane)

Basic object in string-theory, the geometrical locus of open string endpoints

Has a tension

Geometric characterization of a brane

Intrinsic geometry

=induced metric (1st fundamental form)

=tensorial degrees of freedom of gravity

Embedding properties

=extrinsic curvature (2nd fundamental form)

one for each normal

(simplest model: co-dimension 1)

(tip of the cone: co-dimension 2, etc)

=additional sources of gravity

ADM for brane-worlds

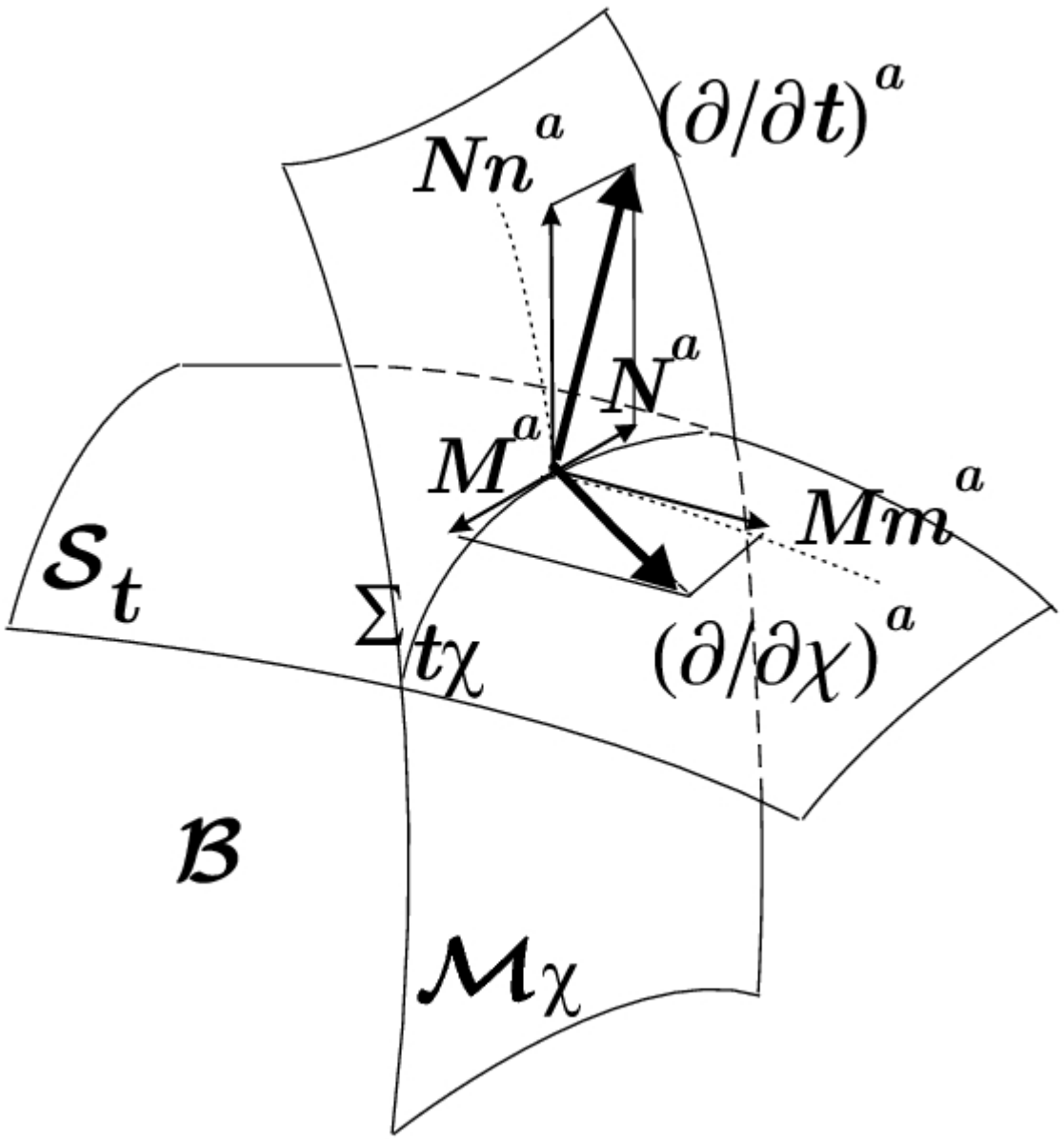

LÁ Gergely, Z Kovács
Phys. Rev. D 72,
064015-1-12 (2005)

Z Kovács, LÁ Gergely
Phys. Rev. D 77,
024003-1-13 (2008)

Junction conditions across the brane (Israel-Lanczos)

Continuity of the induced metric required

Continuity of the extrinsic curvature not required
→ the brane may look differently from the two sides

The jump (discontinuity) in the extrinsic curvature is related to the (distributional) energy-momentum tensor on the brane (Lanczos equation)

Analogous with:

jump in tangential magnetic field → surface current

jump in normal electric field → surface charge

Resembling shock waves

Covariant dynamics

5D Einstein eq. $\tilde{G}_{ab} = \tilde{\kappa}^2[-\tilde{\Lambda}\tilde{g}_{ab} + \tilde{T}_{ab} + \tau_{ab}\delta(y - y_b)]$

$$\tau_{ab} = -\lambda g_{ab} + T_{ab}$$

Decomposition w.r.to the brane normal n^a : $\tilde{g}_{ab} = n_a n_b + g_{ab}$

Sum and difference equations of the projections of the 5D Einstein:

- vectorial: ⟷ averaged Codazzi + energy balance
- tensorial – trace → twice contacted Gauss
  – trace-free → effective Einstein eq. + embedding constr.
- scalar → + eq. for $\Delta\mathcal{E}_{ab}$

electric projection of the Riemann tensor replaced by electric part of the Weyl tensor $\mathcal{E}_{ab}$

extrinsic curvature terms replaced by brane sources (Lanczos) and embedding terms

The tidal charged black holes

Tidal charged BH:

- symmetric embedding,
- 4D and 5D vacuum,
- spherical symmetry.

Dadhich, Maartens, Papadopoulos, Rezania, Phys. Lett B 487, 1 (2000)

$$ds^2 = -f(r)\,dt^2 + f^{-1}(r)\,dr^2 + r^2\left(d\theta^2 + \sin^2\theta d\varphi^2\right)$$

$$f(r) = 1 - \frac{2m}{r} + \frac{q}{r^2}$$

q>0

- analogy with charged RN
- two horizons inside the Schwarzschild radius
- gravity on the brane is weakened

q<0

- no analogue in GR
- one horizon outside the Schwarzschild radius
- brane gravity is strengthened / confinement of gravity to the brane

horizon(s): $r_\pm = m \pm \Theta\,, \qquad \Theta = \sqrt{m^2 - q}$

5D extension unknown

BUT proven to exist in certain parameter range

1 Image formation in weak gravitational lensing by tidal charged black holes

To second order in the small parameters: $\varepsilon = \frac{m}{b}\,, \qquad \eta = \frac{q}{b^2}$

by a Lagrangian method: **LÁ Gergely, B Darázs: astro-ph/0602427 (2006)**

$$\delta\varphi = \frac{4m}{r_{\min}} - \frac{3\pi q}{4r_{\min}^2} + \frac{(15\pi-16)m^2}{4r_{\min}^2} + \frac{57\pi q^2}{64r_{\min}^4} + \frac{(3\pi-28)mq}{2r_{\min}^3}\,.$$

confirmed by a Hamiltonian method (eikonal equation):

LÁ Gergely, Z Keresztes, M Dwornik: Class. Quantum Grav. 26, 145002 (2009)

Lensing images:

Z Horváth, LÁ Gergely, D Hobill: Class. Quantum Grav. 27, 235006 (2010)

- small tidal charge: 2 images, Einstein ring (Schwarzschild lensing)
- small mass: Schwarzschild-like lensing for $q<0$

  2, 1 or 0 images, no ring for $q>0$

Image formation in weak gravitational lensing by tidal charged black holes

Image positions

(mass dominated case)

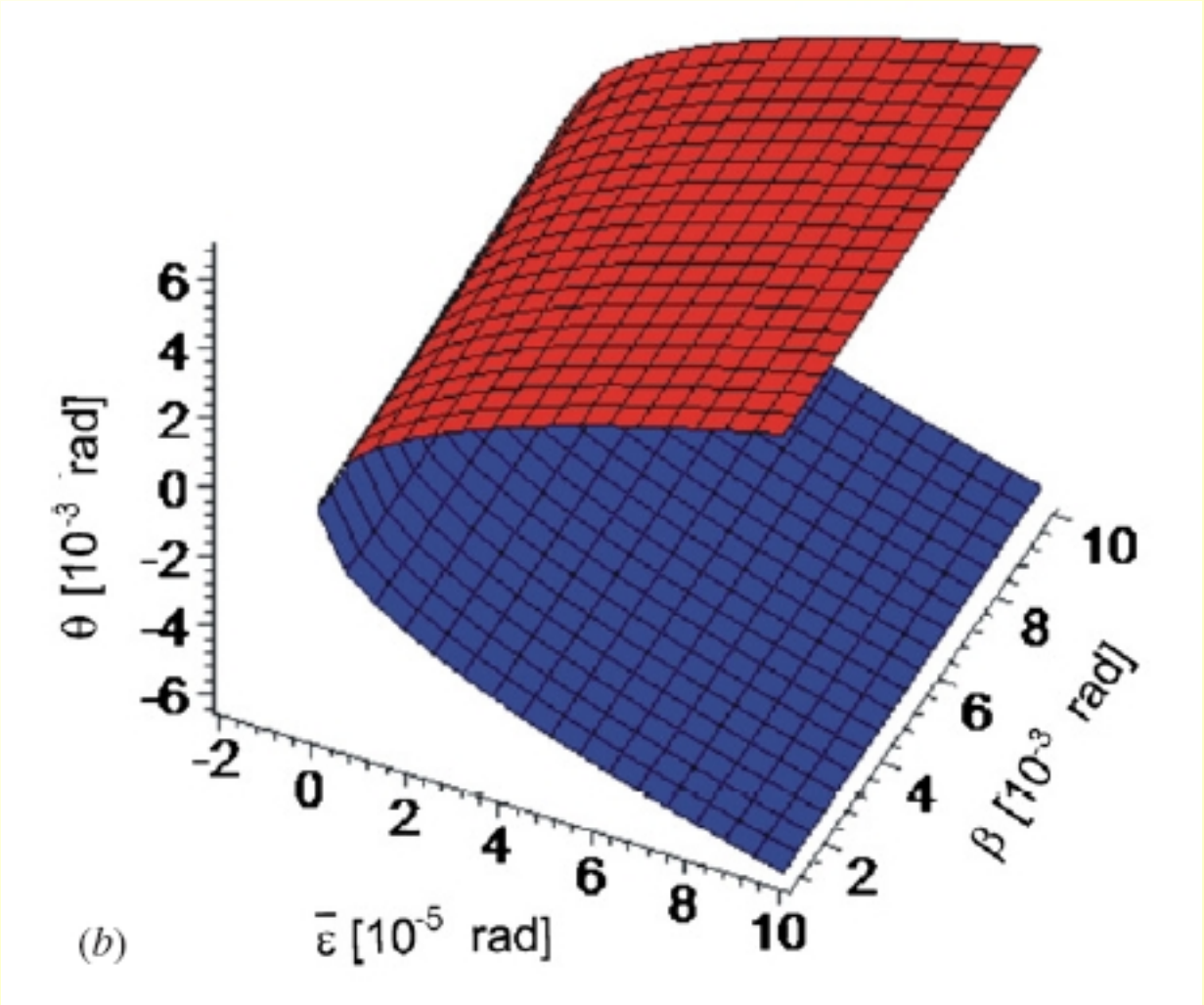

Image positions (tidal charge dominated case)

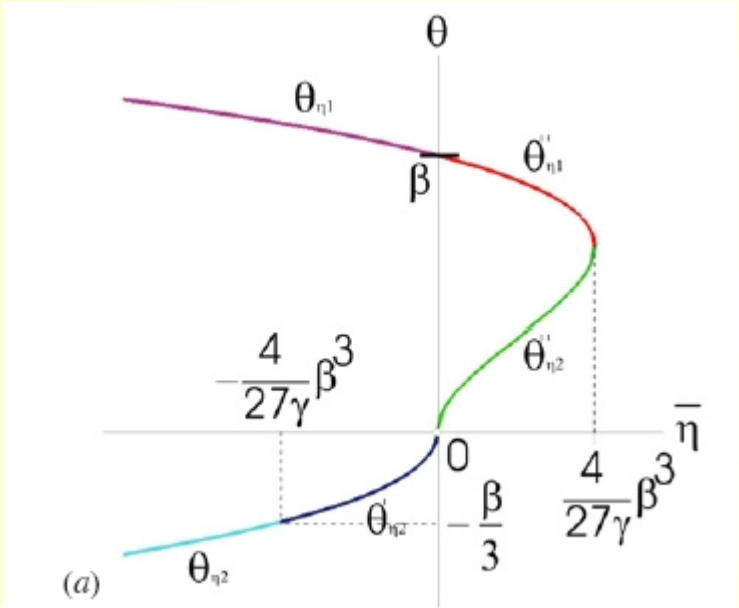

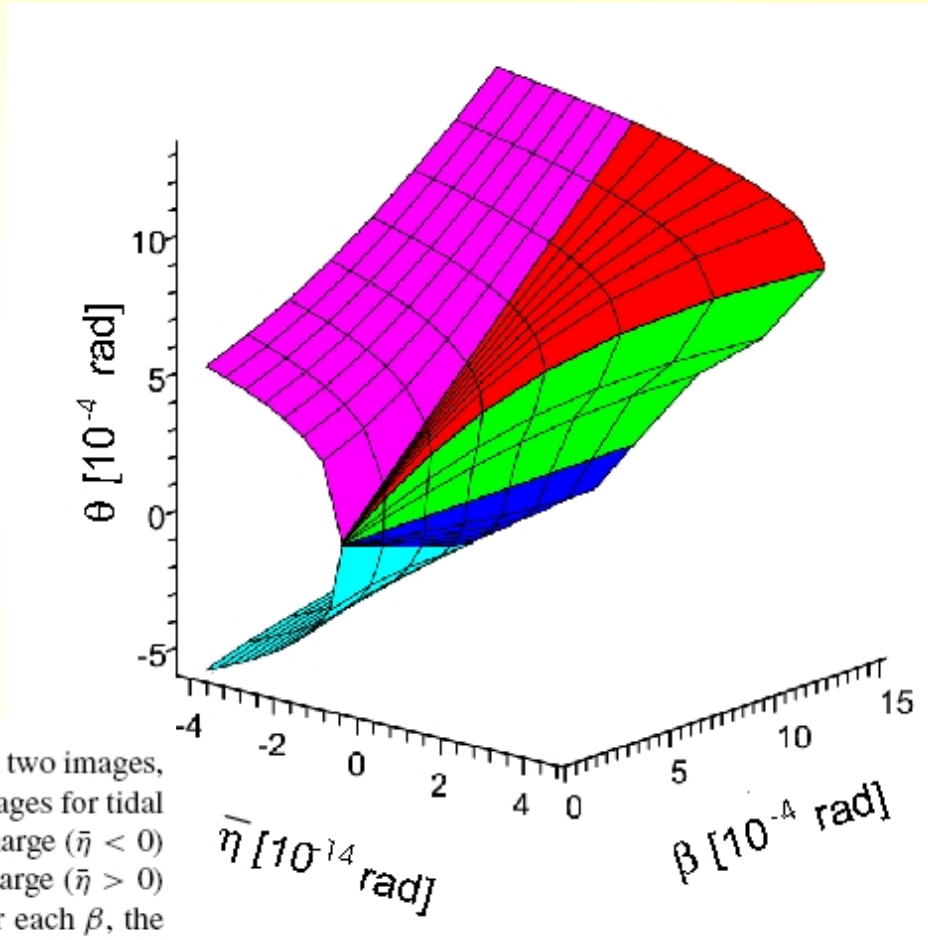

Figure 4. When the tidal charge dominates over the mass in the lensing, there are still two images, but different from the Schwarzschild case. (*a*) The position θ (in units of β) of the images for tidal charge-dominated black holes characterized by the parameter $\bar{\eta}$. For negative tidal charge ($\bar{\eta} < 0$) there are two images, situated above and below the optical axis. For positive tidal charge ($\bar{\eta} > 0$) both images lie above the optical axis. The images coincide for $\bar{\eta} = 4\beta^3/27\gamma$. For each β, the positive tidal charges with $\bar{\eta} > 4\beta^3/27\gamma$ do not allow for any image. The colors distinguish the images obtained as distinct analytic expressions, which however generate a globally continuous curve. (*b*) θ as function of $\bar{\eta}$ and β. With decreasing β, the images shrink accordingly. At $\beta = 0$,the angle θ represents the angular radius of the Einstein ring (therefore, the $\beta = 0$ section of the surface is symmetric with respect to $\theta = 0$).

Image formation in weak gravitational lensing by tidal charged black holes

Magnifications

(mass dominated case)

$$\mu = \left| \frac{\theta}{\beta} \frac{\mathrm{d}\theta}{\mathrm{d}\beta} \right|$$

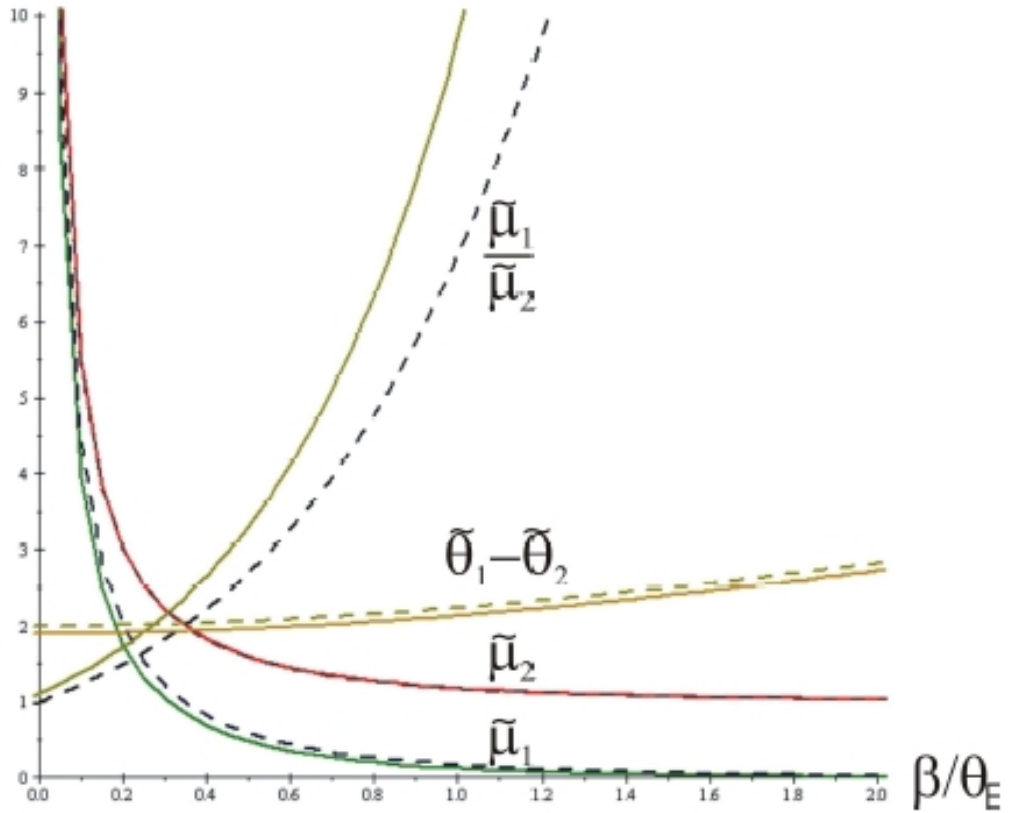

Figure 3. (Colour online.) The image separations, the magnifications of the two images and their ratio as functions of β/θ_E for the perturbed case (solid lines) as compared to the Schwarzschild case (dashed lines) for the parameter values $\gamma\left(\bar{\eta}-5\bar{\varepsilon}^2\right) = 10^{-1}\theta_E^3$. From top to bottom at $\beta/\theta_E = 0.8$ they are the flux ratio $\tilde{\mu}_1/\tilde{\mu}_2$, the image separation $\tilde{\theta}_1 - \tilde{\theta}_2$, the magnification of the primary image $\tilde{\mu}_1$ and finally the magnification of the secondary image $\tilde{\mu}_2$. The largest effect can be seen on the flux ratios.

Image formation in weak gravitational lensing by tidal charged black holes

Magnifications

(negative tidal charge dominated case)

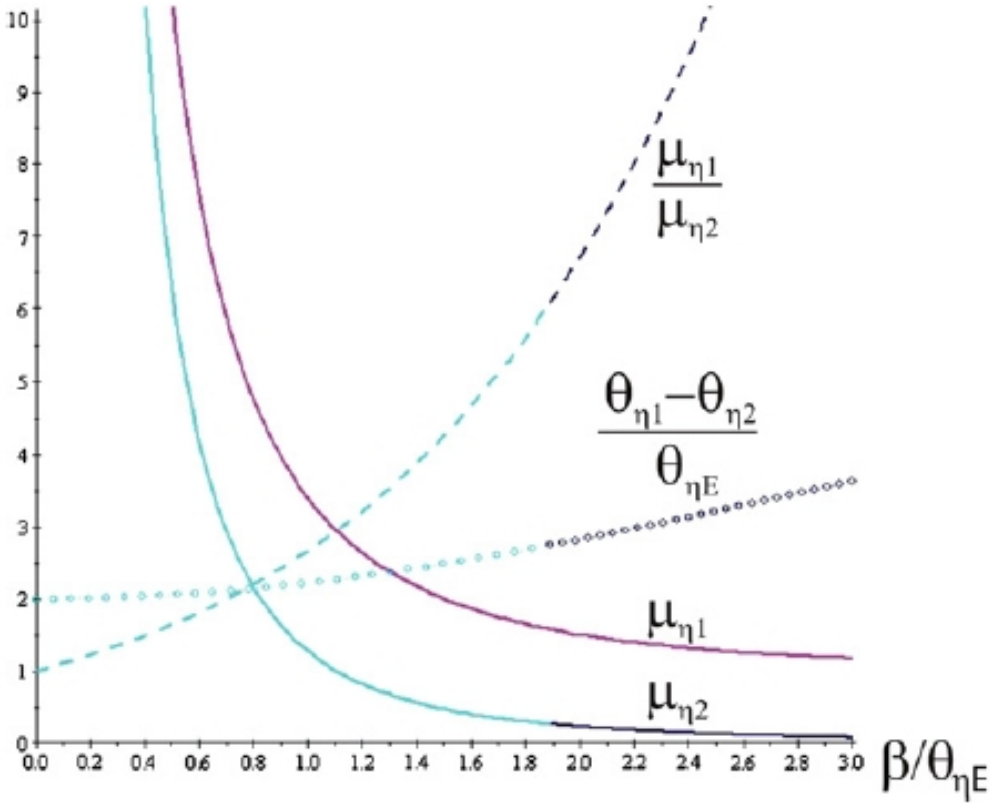

Figure 5. Image separations and magnifications for a negative tidal charge-dominated black hole, as functions of $\beta/\theta_{\eta E}$. The upper and lower solid curves plot the primary and secondary image magnification factors, respectively; their ratio is the dashed curve; and the dotted curve is the image separation. A color change at $3/4^{1/3}$ represents the change in functional form from $\theta_{\eta 2}$ (left) to $\theta'_{\eta 2}$ (right).The colors match those of figure 4.

1 Image formation in weak gravitational lensing by tidal charged black holes

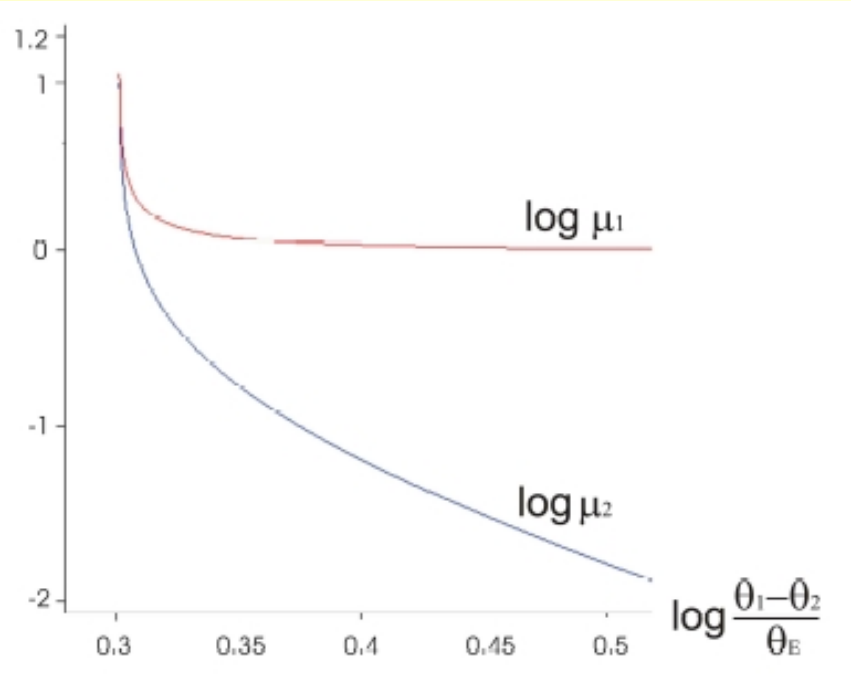

Mass dominated

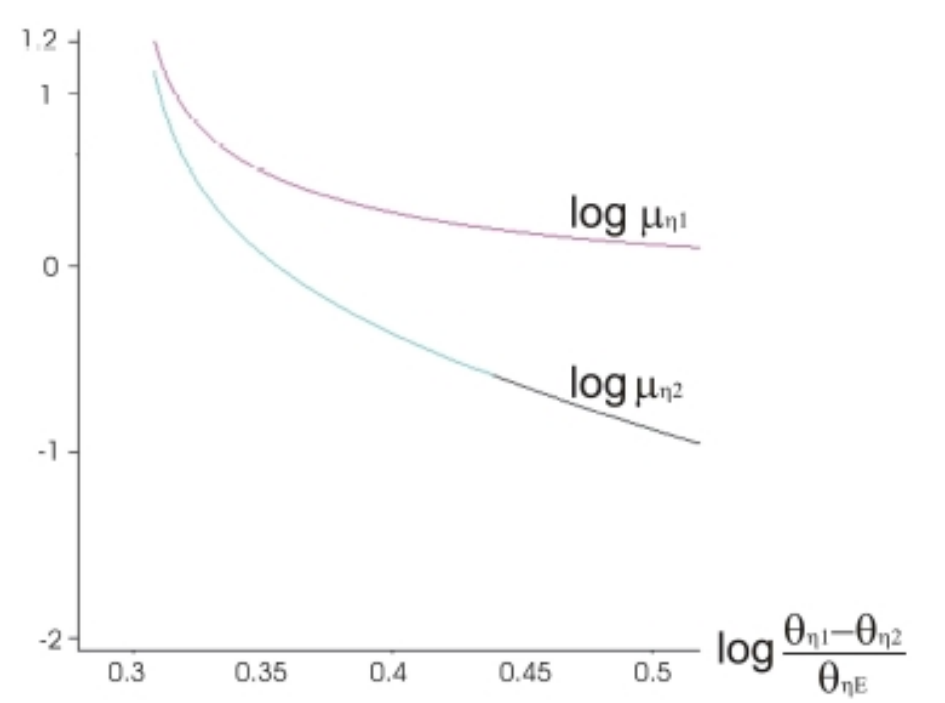

Negative tidal charge dominated

The power law dependence of the magnification factors on the separation of the images provides a significant difference in the two cases.

Image formation in weak gravitational lensing by tidal charged black holes

- observable signature

for large image separations one has

$$\mu_1/\mu_2 \approx [\Delta\theta/\theta_E]^{\kappa}.$$

Schwarzschild lensing $\kappa = 6.22 \pm .15$

tidally charged black hole lensing $\kappa_\eta = 2.85 \pm .25$

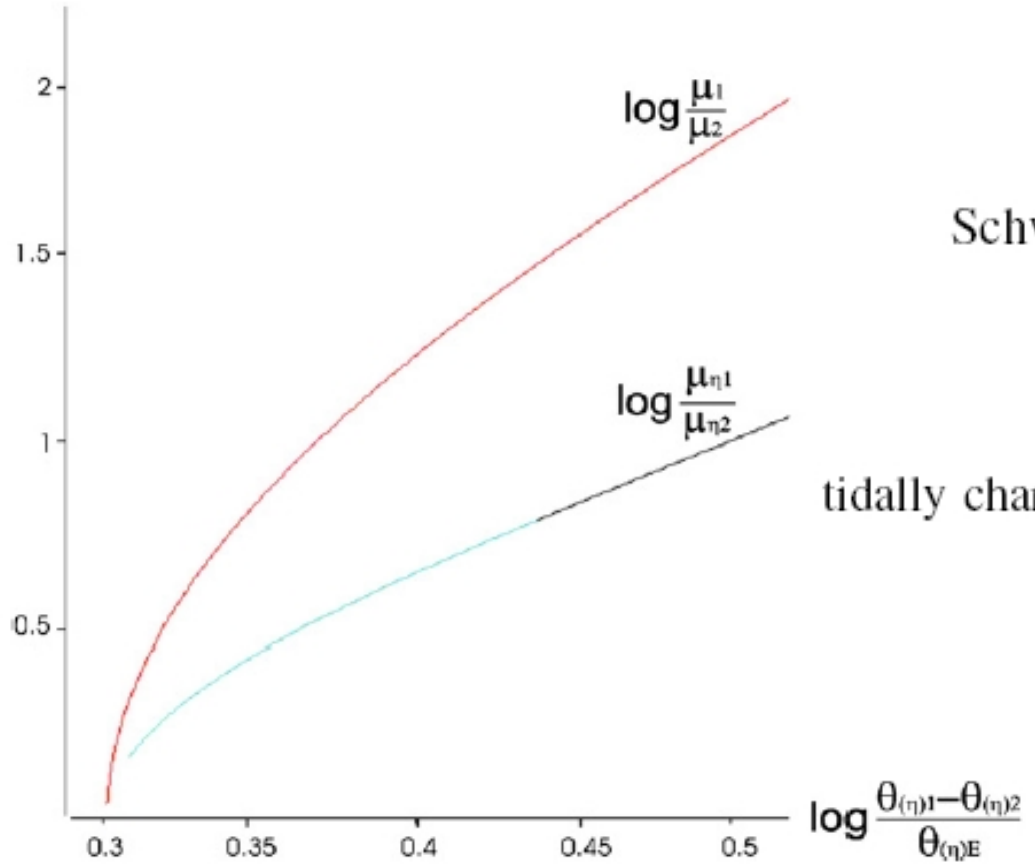

Figure 6. The ratio of the magnification factor of the primary and secondary images as function of the image separation normalized to the Einstein angle, on the log–log scale, for the tidal charge-dominated black hole and Schwarzschild black hole. The tidal charged case is distinguished by the use of the η-subscript.

Testing the dark radiation dominated region of braneworld models with gravitational lensing

KC Wong, T Harko, KS Cheng, LÁ Gergely, Phys. Rev. D **86**, 044038-1-15 (2012)

- spherically symmetric sol. of vacuum effective Einstein eq.

$$ds^2 = -e^{\nu(r)}dt^2 + e^{\lambda(r)}dr^2 + r^2 d\Omega^2,$$

- metric functions in the weak field limit

$$e^{\nu(r)} \approx 1 - \frac{2GM_1}{c^2 r} + \frac{2\gamma}{1-\alpha}\left(\frac{r}{r_c}\right)^{\alpha-1},$$

$$e^{-\lambda(r)} \approx 1 - \frac{2GM_1}{c^2 r} + \gamma\left[\left(\frac{r}{r_c}\right)^{\alpha-1} - 1\right],$$

- equation of state of the Weyl fluid (dark pressure + radiation)

$$P = (a-2)\,U - \frac{B}{3\alpha_b r^2},$$

Testing the dark radiation dominated region of braneworld models with gravitational lensing

- fixing the parameters from galactic rotation curves

LÁ Gergely, T Harko, M Dwornik, G Kupi, Z Keresztes:
Mon. Not. Royal Astron. Soc. 415, 3275-3290 (2011)

[arXiv:1105.0159 [gr-qc]]

Galaxy	M_1	r_c	α	γ	$\chi^2_{\rm min}$
	$M_\odot$	kpc			
DDO 189	4.05×10^8	1.25	0.3	6.43×10^{-8}	0.742
NGC 2366	1.05×10^9	1.47	0.8	1.12×10^{-7}	2.538
NGC 3274 1	4.38×10^8	0.69	-0.4	6.73×10^{-8}	18.099
NGC 4395	2.37×10^8	0.71	0.9	3.43×10^{-7}	27.98
NGC 4455	2.26×10^8	1.03	0.9	2.72×10^{-7}	7.129
NGC 5023	2.69×10^8	0.74	0.9	4.53×10^{-7}	10.614
UGC 10310	1.28×10^9	2.6	0.4	1.12×10^{-7}	0.729
UGC 1230	3.87×10^9	3.22	-1.7	1.12×10^{-7}	0.539
UGC 3137	5.32×10^9	3.87	-0.5	1.23×10^{-7}	4.877

The best fit parameters of the 9 LSB galaxy sample (M_0, r_c, α, γ)

Testing the dark radiation dominated region of braneworld models with gravitational lensing

- deflection angle

$$\delta\left(r_{\min}\right) = 2\int_{r_{\min}}^{\infty} \mathcal{I} dr - \pi,$$

$$\mathcal{I}\left(r\right) = \frac{1}{r}\left\{\frac{g_{rr}\left(r\right)}{\left[\left(-g_{tt}\left(r_{\min}\right)\right)/\left(-g_{tt}\left(r\right)\right)\right]\left(r/r_{\min}\right)^{2}-1}\right\}^{1/2}$$

- expansion in the PN parameter and brane parameter γ

$$\mathcal{I} = \mathcal{I}_0 + \mathcal{I}_S + \mathcal{I}_W \ ,$$

$$\mathcal{I}_0 = \frac{1}{r}\sqrt{\frac{1}{u^2-1}}$$

$$\mathcal{I}_S = \varepsilon\left(\frac{1+u+u^2}{1+u}\right)\mathcal{I}_0$$

$$\mathcal{I}_W = \frac{\gamma}{2}\left[1+\left(\frac{r_{\min}}{r_c}\right)^{\alpha-1}\frac{(1-\alpha)u^{\alpha-1}+(1+\alpha)u^{\alpha+1}-2u^2}{(1-\alpha)\left(u^2-1\right)}\right]\mathcal{I}_0 \ .$$

can the brane effects cancel?

Testing the dark radiation dominated region of braneworld models with gravitational lensing

- critical behaviour

- Lensing amplified outside the critical radius, reduced inside

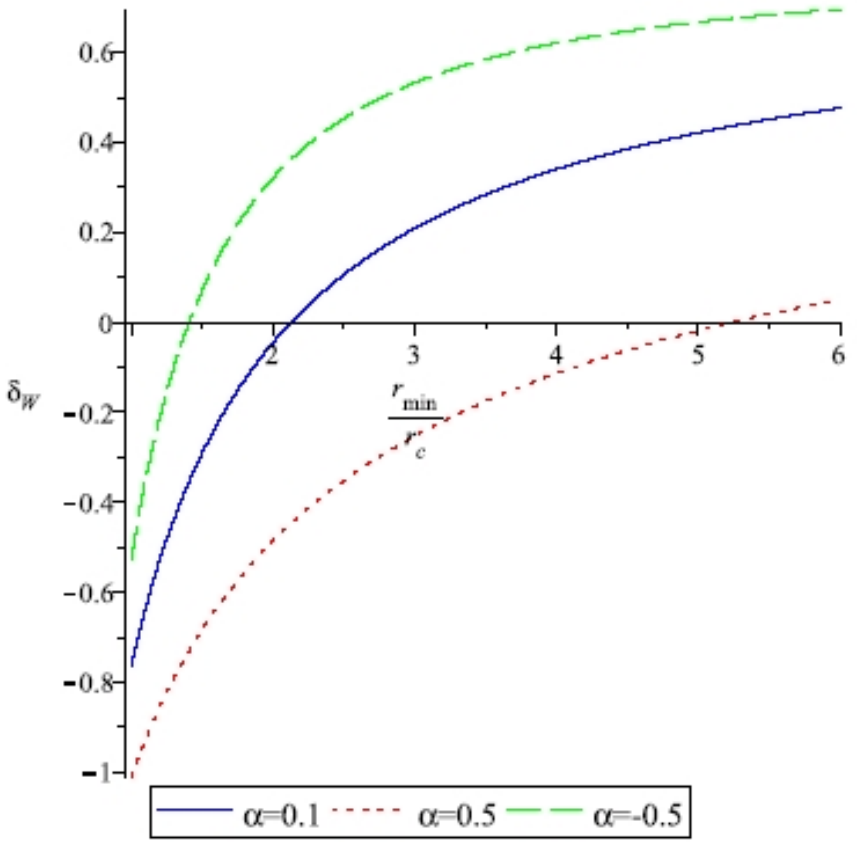

FIG. 3: The plot shows the evolution of the braneworld contribution δ_W to the deflection angle, as function of $r_{\rm min}/r_c$ for various values of the braneworld parameter α. The contribution δ_W is positive for orbits with the closest approach $r_{\rm min}$ above the critical radius $r_{\rm min}^{crit}$ (defined by the intersection with the horizontal axis).

[7] P. Hořava, "Quantum gravity at a Lifshitz point", Phys. Rev. **D79** (2009) 084008. [arXiv:0901.3775 [hep-th]].
[8] P. Hořava, "Membranes at quantum criticality", JHEP **0903** (2009) 020. [arXiv:0812.4287 [hep-th]].
[9] P. Hořava, "Spectral dimension of the universe in quantum gravity at a Lifshitz point", Phys. Rev. Lett. **102** (2009) 161301. [arXiv:0902.3657 [hep-th]].

Status of Hořava gravity: A personal perspective

Matt Visser

School of Mathematics, Statistics, and Operations Research
Victoria University of Wellington
Wellington, New Zealand

E-mail: matt.visser@msor.vuw.ac.nz

Abstract. Hořava gravity is a relatively recent (Jan 2009) idea in theoretical physics for trying to develop a quantum field theory of gravity. It is not a string theory, nor loop quantum gravity, but is instead a traditional quantum field theory that breaks Lorentz invariance at ultra-high (presumably trans-Planckian) energies, while retaining approximate Lorentz invariance at low and medium (sub-Planckian) energies. The challenge is to keep the Lorentz symmetry breaking controlled and small — small enough to be compatible with experiment. I will give a very general overview of what is going on in this field, paying particular attention to the disturbing role of the scalar graviton.

HL gravity:

- renormalizable field theoretical model
- IR energy scales, Einstein gravity with a nonvanishing cosmological constant
- UV energy scales: anisotropic Lifshitz scaling between time and space $x^i \to l x^i$, $t \to l^z t$
- massive particles do not, massless particles do follow geodesics!

Hořava-Lifshitz gravity

J Greenwald, J Lenells, JX Lu, VH Satheeshkumar, A Wang, Phys. Rev. D 84, 084040 (2011)

Three major problems, ghosts, strong coupling and instability, of the same origin: the breaking of the general covariance

The preferred time that breaks general covariance leads to a reduced set of diffeomorphisms → a spin-0 graviton appears →instability, ghost and strong coupling problems, which could prevent the recovery of GR in the IR

Various modications proposed.

1. introduce a vector, the gradient of the lapse logarithm

2. extend the diff invariance with local U(1) → scalar graviton eliminated

....

Hořava-Lifshitz gravity

Action:

$$S = \int dt\, d^3x\, \sqrt{g} N \left[\frac{2}{\kappa^2} \left(K_{ij} K^{ij} - \lambda_g K^2 \right) - \frac{\kappa^2}{2\nu_g^4} C_{ij} C^{ij} + \frac{\kappa^2 \mu}{2\nu_g^2} \epsilon^{ijk} R^{(3)}_{il} \nabla_j R^{(3)l}{}_k \right.$$
$$\left. - \frac{\kappa^2 \mu^2}{8} R^{(3)}_{ij} R^{(3)ij} + \frac{\kappa^2 \mu^2}{8(3\lambda_g - 1)} \left(\frac{4\lambda_g - 1}{4} (R^{(3)})^2 - \Lambda_W R^{(3)} + 3\Lambda_W^2 \right) + \frac{\kappa^2 \mu^2 \omega}{8(3\lambda_g - 1)} R^{(3)} \right]$$

Cotton-York tensor:

$$C^{ij} = \epsilon^{ikl} \nabla_k \left(R^{(3)j}{}_l - \frac{1}{4} R^{(3)} \delta^j_l \right)$$

Constants:

$$c^2 = \frac{\kappa^2 \mu^2 |\Lambda_W|}{8(3\lambda_g - 1)^2}, \quad G = \frac{\kappa^2 c^2}{16\pi (3\lambda_g - 1)}, \quad \Lambda = \frac{3}{2} \Lambda_W c^2$$

GR limit:

$\lambda_g = 1$, which reduces to the Einstein-Hilbert action in the IR limit.

- spherically symmetric BH: Kehagias-Sfetsos asymptotically flat space-time

$$ds^2 = g_{tt}(r)dt^2 + g_{rr}(r)dr^2 + r^2(d\Theta^2 + \sin^2\Theta d\varphi^2),$$

$$-g_{tt}(r) = 1/g_{rr}(r) = 1 + \omega r^2\left[1 - \left(1 + \frac{4GM}{c^2\omega r^3}\right)^{1/2}\right]$$

- event horizon

$$r_{\pm} = m\left(1 \pm \sqrt{1 - \frac{1}{2\omega_0}}\right) \qquad \omega_0 = m^2\omega$$

BUT: difficulties related to the black hole interpretation due to the nonrelativistic dispersion relations!

Z Horváth, LÁ Gergely, Z Keresztes, T Harko, FSN Lobo

Phys Rev. D 84, 083006-1-9 (2011) *[arXiv:1105.0765 [gr-qc]]*

- deflection angle

$$\delta(x_0) = 2\int_0^{\pi/2}\left[1 + \frac{8(\sin^3\alpha - 1)(\tan^2\alpha + 1)\omega_0 x_0}{(16\omega_0^2 x_0^4 + 8\omega_0 x_0 \sin^3\alpha)^{1/2} + (16\omega_0^2 x_0^4 + 8\omega_0 x_0)^{1/2}}\right]^{-1/2} d\alpha - \pi.$$

When $\omega_0 \to \infty$ we obtain the Schwarzschild limit of the deflection angle, increasing with $x_0 = r_{\min}/2m$ (the distance of closest approach to the lensing object). By contrast, the limit $\omega_0 \to 0$ gives a flat space-time and a vanishing deflection angle. With no lens mass there is also no deflection, irrespective of the value of ω, as ω_0 vanishes. The quantities m, x_0, and $\delta(x_0)$ have all the same sign, as in Schwarzschild lensing.

- small parameters for weak lensing

$$\bar{\lambda} = 1/\omega d^2 \qquad \bar{\varepsilon} = m/d$$

- Einstein ring radius

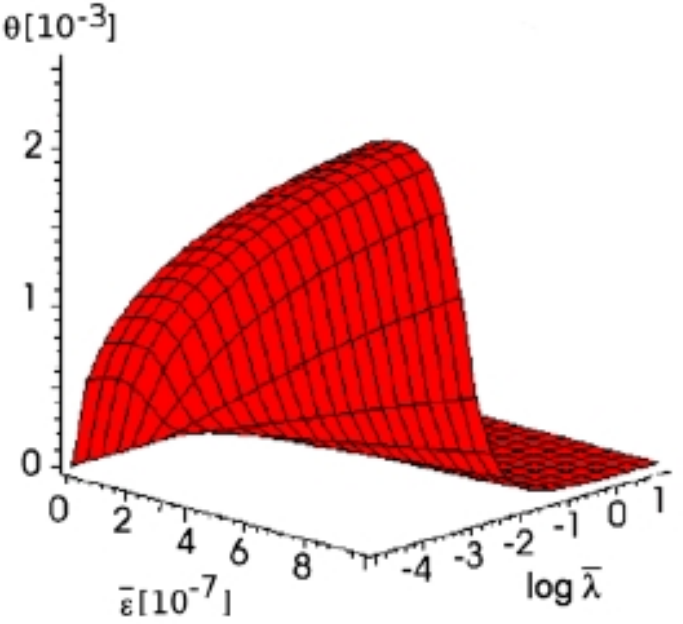

FIG. 2 (color online). The radius of the Einstein ring as function of the mass parameter $\bar{\varepsilon}$ and Hořava-Lifshitz parameter $\bar{\lambda}$ for the Kehagias-Sfetsos space-time, assuming $D_{LS}/D_L = 2$. For $\bar{\lambda} \to 0$, we reobtain the Schwarzschild result. With increasing $\bar{\lambda}$, as the metric approaches flatness, the radius of the Einstein ring shrinks, and tends to zero for large values of $\bar{\lambda}$.

- Image positions

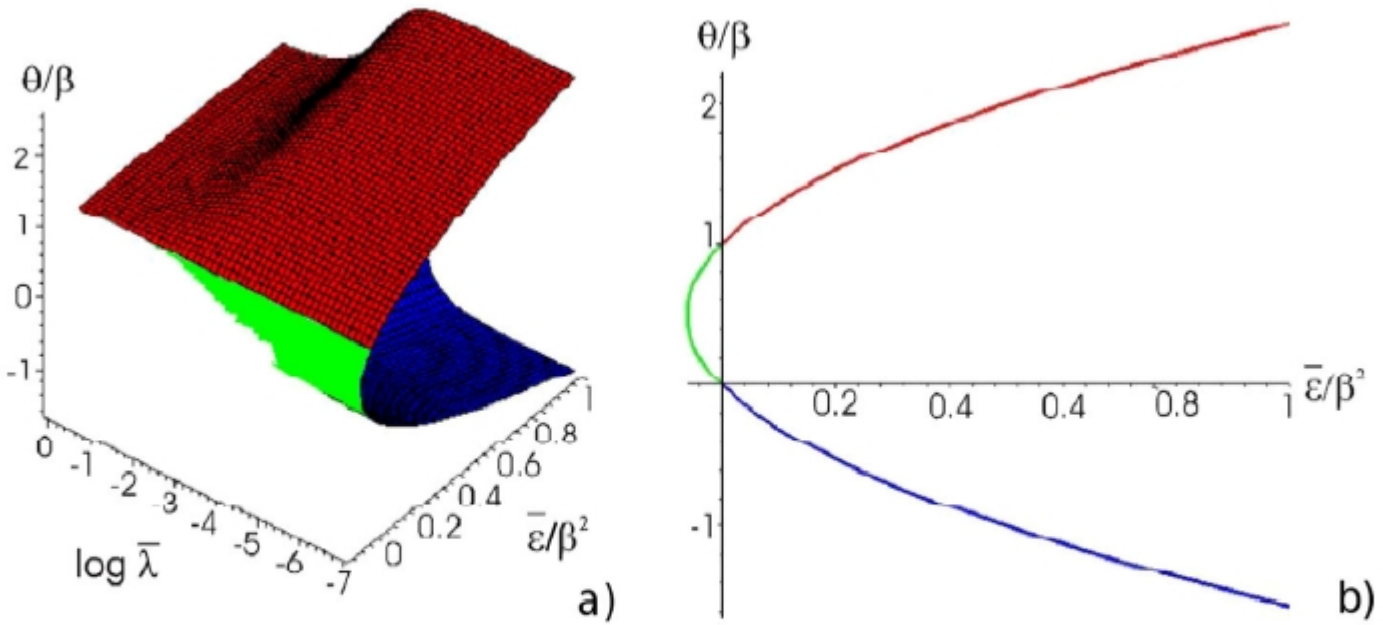

FIG. 3 (color online). The position of the images as function of the mass parameter $\bar{\varepsilon}$ and Hořava-Lifshitz parameter $\bar{\lambda}$ for the Kehagias-Sfetsos space-time (with $D_{LS}/D_L = 2$ and $\beta = 10^{-3}$ rad) is represented on panel (a). The three surfaces on the figure refer to: (1) the focused positive image is represented by the upper (red) surface; (2) the focused negative image is seen underneath (blue); (3) the scattered images (with $0 < \theta < \beta$) are found in the junction of the two surfaces mentioned generated by a negative mass (green). For $\bar{\lambda} \to 0$ we reobtain the Schwarzschild result, the parabola shown on panel (b). With increasing $\bar{\lambda}$ only the positive focused image is left. For very large $\bar{\lambda}$, the metric approaches flatness.

- another critical value: with the exception of the Schwarzschild limit, there is a maximum of the deflection angle, trajectories both with larger and smaller impact parameters exhibiting less deflection

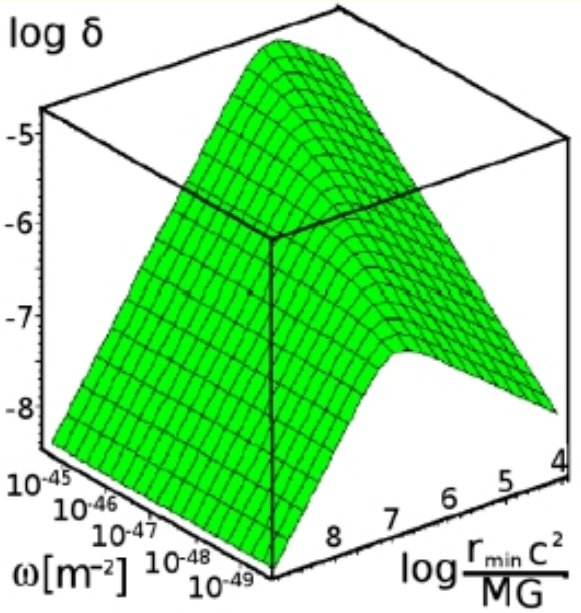

FIG. 4 (color online). The logarithm of the deflection angle δ as a function of the distance of minimal approach (represented in units m, on logarithmic scale) and Hořava-Lifshitz parameter ω. The represented range of ω corresponds to the range of $\bar{\lambda}$ of Fig. 3, when the lens mass is $m = 4.284 \cdot 10^{14}$ meter, $D_S = 4.190 \cdot 10^{25}$ meter, and $D_{LS}/D_L = 2$. For every ω there is a maximal deflection angle $\delta_{\max}$, corresponding to certain r_{crit}. The critical r_{crit} distance decreases with increasing ω. (Near the Schwarzschild limit r_{crit} shelters below the horizon and tends to 0 when $\omega \to \infty$, resulting in the well-known decreasing $\delta(r_{\min})$ function out of the horizon.) Rays passing both above and below r_{crit} will experience less deflection than $\delta_{\max}$.

- photometric and spectroscopic measurements for a sample of 57 SDSS lens galaxies → observed locations of the corresponding Einstein rings → range of the HL parameter determined

TABLE I. Column 1: the lens galaxies. Column 2–5: the Einstein angle θ_E, total lens mass inside the Einstein radius R_E, the distances D_L and D_{LS}. The quantities calculated from the model are r_{min} (Column 6), ω_{min} and $\omega_{0,min} := G^2 M^2_{lum+dark} \omega_{min}/c^4$ (Columns 7 and 8).

galaxy	θ_E [arcsec]	M $[10^{10} M_\odot]$	D_L [Mpc]	D_S [Mpc]	r_{min} [Kpc]	$\omega_{min}[10^{-48}$ cm$^{-2}]$	$\omega_{0,min}$
J0008 − 0004	1.16	35	1172.743	1708.956	6.595	0.189 42	5.0657
J0029 − 0055	0.96	12	750.391	1622.253	3.492	0.270 33	0.849 82
J0037 − 0942	1.53	29	669.889	1411.834	4.969	0.346 28	6.3576
J0044 + 0113	0.79	9	446.200	672.576	1.709	1.2219	2.1606
J0109 + 1500	0.69	13	905.964	1291.699	3.031	0.334 25	1.2332
J0157 − 0056	0.79	26	1276.277	1618.923	4.888	0.237 49	3.5047
J0216 − 0813	1.16	49	984.161	1289.158	5.535	0.356 70	18.697
J0252 + 0039	1.04	18	875.400	1644.710	4.414	0.228 16	1.6138
J0330 − 0020	1.10	25	1020.790	1676.984	5.444	0.200 53	2.7361
J0405 − 0455	0.80	3	293.680	1555.222	1.139	1.1703	0.229 93
J0728 + 3835	1.25	20	696.489	1463.700	4.221	0.321 41	2.8066
J0737 + 3216	1.00	29	964.236	1358.283	4.675	0.303 24	5.5673
J0822 + 2652	1.17	24	784.904	1372.544	4.452	0.309 91	3.8969
J0903 + 4116	1.29	45	1157.167	1675.061	7.237	0.197 36	8.7248
J0912 + 0029	1.63	40	580.506	968.258	4.587	0.604 97	21.131
J0935 − 0003	0.87	41	1013.21	1213.066	4.274	0.483 86	17.756
J0936 + 0913	1.09	15	653.631	1366.016	3.454	0.366 99	1.8026
J0946 + 1006	1.38	29	737.793	1388.471	4.936	0.320 25	5.879 66

- … more galaxies ….

- other constraints for ω_0

Solar System:

Perihelion precession of the planet Mercury $\omega_{0,\min}^{(pp)} = 6.9 \times 10^{-16}$

Deflection of light by the Sun $\omega_{0,\min}^{(ld)} = 1.1 \times 10^{-15}$

radar echo delay $\omega_{0,\min}^{(\mathrm{red})} = 2 \times 10^{-15}$

orbital periods of the transiting extrasolar planet HD209458b (Osiris)

$\omega_0^{(\mathrm{Osiris})} = 1.4 \times 10^{-18}$

light deflection observations including long-baseline radio interferometry, Jupiter measurement, and the Hipparcos satellite $\omega_0^{(\mathrm{radio})} \in 10^{-15} \div 10^{-17}$

range-residuals of the system constituted by the S2 star orbiting the supermassive black hole (Sagittarius A) in the center of the Galaxy

$\omega_0^{(\mathrm{Sag})} = 8 \times 10^{-10}$

- strong lensing

TABLE III. Radii of the first and second relativistic Einstein rings, with corresponding $\omega_{\min}$ and $\omega_{0,\min}$ for $\Delta\theta_E = 10^{-5}$ arcsec.

Einstein ring	$\theta_{E,Sch}\,[10^{-5}\text{arcsec}]$	$\omega_{\min}[\text{cm}^{-2}]$	$\omega_{0,\min}$
1st relativistic	2.557	$8.1315 \cdot 10^{-25}$	0.3282
2nd relativistic	2.554	$8.1315 \cdot 10^{-25}$	0.3282

Finally, we discussed the first two relativistic Einstein rings in the strong lensing regime. Applying to the galactic center as a strong lens and a light source located on the opposite side, a configuration discussed in Ref. [23], we determined the constraints on ω_0, given in Table III (under the assumption of fixed lens mass) arising from the expected accuracy of 10^{-5} arcsec of future instruments [22]. We found that such measurements would constrain quite severely the parameter range, up to $\omega_{0,\min}$ of order 10^{-1}, allowing to either falsify the Hořava-Lifshitz theory or to render the parameter of the Kehagias-Sfetsos space-time into a regime where it practically becomes indistinguishable from the Schwarzschild space-time. This would set

from the 10^{-5} arcsec error bar of future instruments

Multi-AO Imaging Camera for Deep Observations (MICADO) – 2018, European Extremely Large Telescope – 42 m

f(R)-gravity

- Generalization of the Hilbert-Einstein action to a generic (unknown) *f(R)* theory of gravity

$$\mathcal{A} = \int d^4x\sqrt{-g}\left[f(R) + \mathcal{L}_{(matter)}\right]$$

$$f'(R)R_{\alpha\beta} - \frac{1}{2}f(R)g_{\alpha\beta} = f'(R)^{;\mu\nu}\left(g_{\alpha\mu}g_{\beta\nu} - g_{\alpha\beta}g_{\mu\nu}\right) + \tilde{T}^{(matter)}_{\alpha\beta}$$

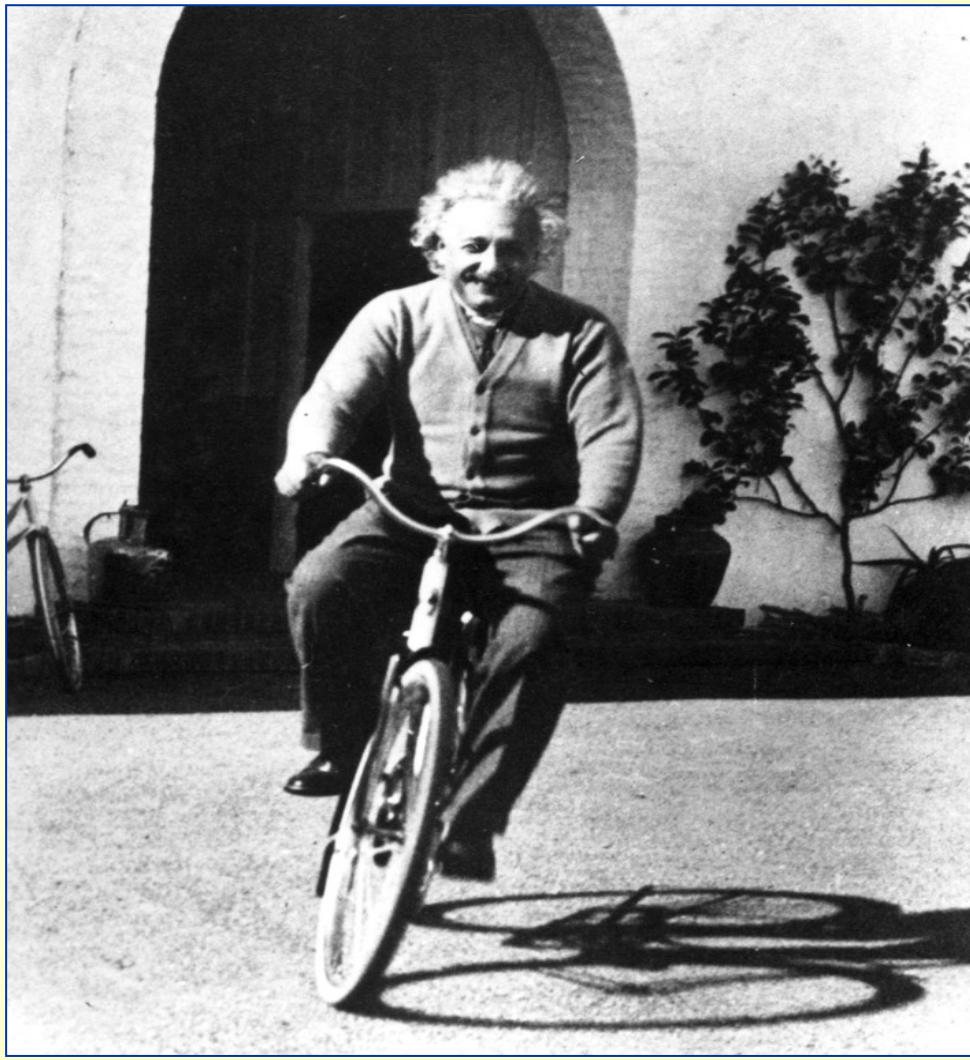

Slide courtesy of Salvatore Capozziello

Theoretical motivations and features:

- Quantization on curved space-time needs higher-order invariants corrections to the Hilbert-Einstein Action.
- These corrections are also predicted by several unification schemes as String/M-theory, Kaluza-Klein, etc.
- A generic action is $\mathcal{A} = \int d^4x\sqrt{-g}\left[F\left(R, \Box R, \Box^2 R, \ldots \Box^k R\right) + \mathcal{L}_m\right]$
- We can consider only fourth order terms *f(R)* which give the main contributions at large scales.
- DE under the standard of FOG inflationary cosmology (Starobinsky) but at different scales and late times.
- This scheme allows to obtain an “Einstein” two fluid model in which one component has a geometric origin

$$G_{\alpha\beta} = R_{\alpha\beta} - \frac{1}{2}g_{\alpha\beta}R = T_{\alpha\beta}^{(curv)} + T_{\alpha\beta}^{(matter)}$$

$$T_{\alpha\beta}^{(curv)} = \frac{1}{f'(R)}\left\{\frac{1}{2}g_{\alpha\beta}\left[f(R) - Rf'(R)\right] + f'(R)^{;\mu\nu}\left(g_{\alpha\mu}g_{\beta\nu} - g_{\alpha\beta}g_{\mu\nu}\right)\right\}$$

Slide courtesy of Salvatore Capozziello

Weak gravitational lensing by fourth order gravity black holes

Zs Horváth, LÁ Gergely, D Hobill, S Capozziello, M de Laurentis arXiv:1207.1823 [gr-qc]

- f(R) gravity

$$\mathcal{A} = \int d^4x\sqrt{-g}\,[f(R) + \mathcal{L}_m]$$

$$G_{\mu\nu} = \frac{1}{f'(R)}\left\{\frac{1}{2}g_{\mu\nu}\,[f(R) - Rf'(R)] + f'(R)_{;\mu\nu} - g_{\mu\nu}\Box f'(R)\right\} + \frac{T^{(m)}_{\mu\nu}}{f'(R)}$$

The simplest choice for $f(R)$ is a power law like $f(R) \propto R^n$

- spherically symmetric BH solution

$$A(r) = \frac{1}{B(r)} = 1 + \frac{2\Phi(r)}{c^2} \qquad \Phi(r;\sigma,r_c) = -\frac{Gm}{2r}\left[1 + \left(\frac{r}{r_c}\right)^{\sigma}\right],$$

$$\sigma = \frac{12n^2 - 7n - 1 - \sqrt{36n^4 + 12n^3 - 83n^2 + 50n + 1}}{6n^2 - 4n + 2}.$$

- deflection angle

$$\delta = \frac{2Gm}{c^2 b}\left[1 + \frac{\sqrt{\pi}(1-\sigma)\Gamma(1-\sigma/2)}{2\Gamma(3/2-\sigma/2)}\left(\frac{b}{r_c}\right)^{\sigma}\right]$$

S Capozziello, V F Cardone, and A Troisi, *Phys. Rev. D* **73** 104019 (2006).

- how the potential differs from Newtonian

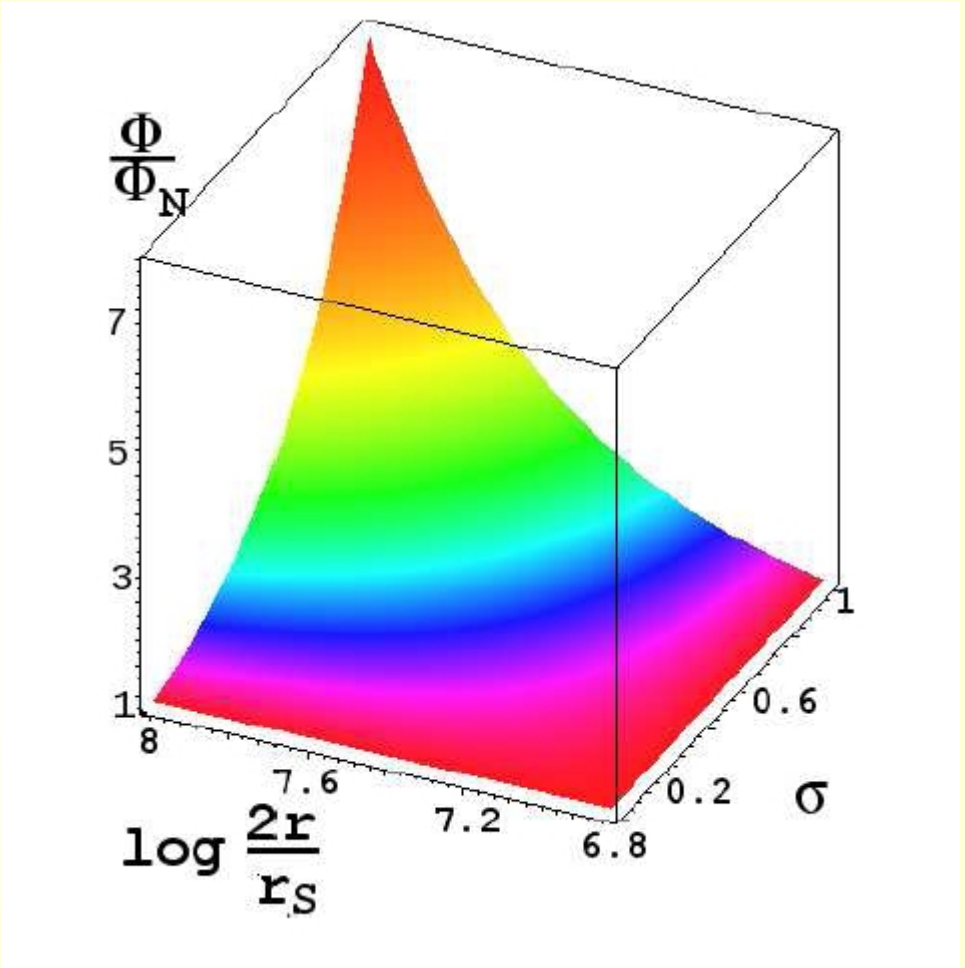

- mimics DM at large distances, when differences w.r.to GR are significant ?

Weak gravitational lensing by fourth order gravity black holes

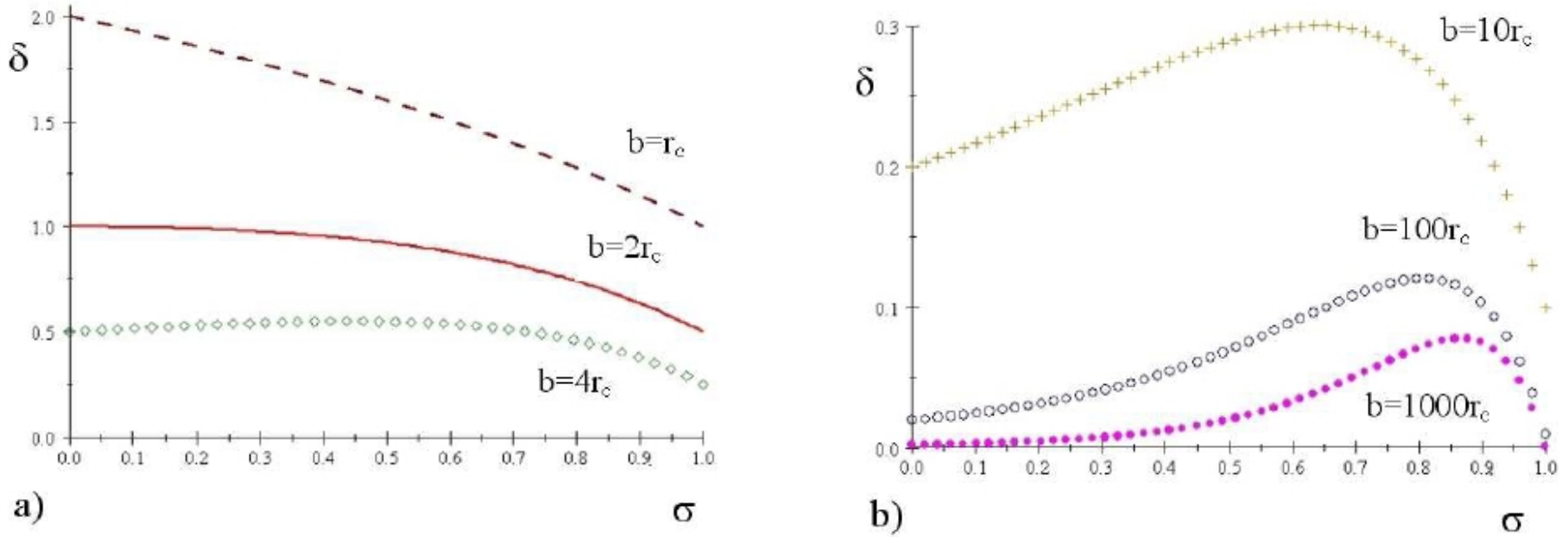

FIG. 5: The plots show the $\delta(\sigma)$ dependence for different values of b/r_c, in units $2Gm/c^2 r_c = 1$. The respective values of b/r_c are from top to bottom 1 (dashed), 2 (solid), 4 (diamond) on panel-a and 10 (cross), 100 (circle), 1000 (dotted) on panel-b. The critical behavior appears at $b/r_c = 2$.

- critical deflection angle

- image positions

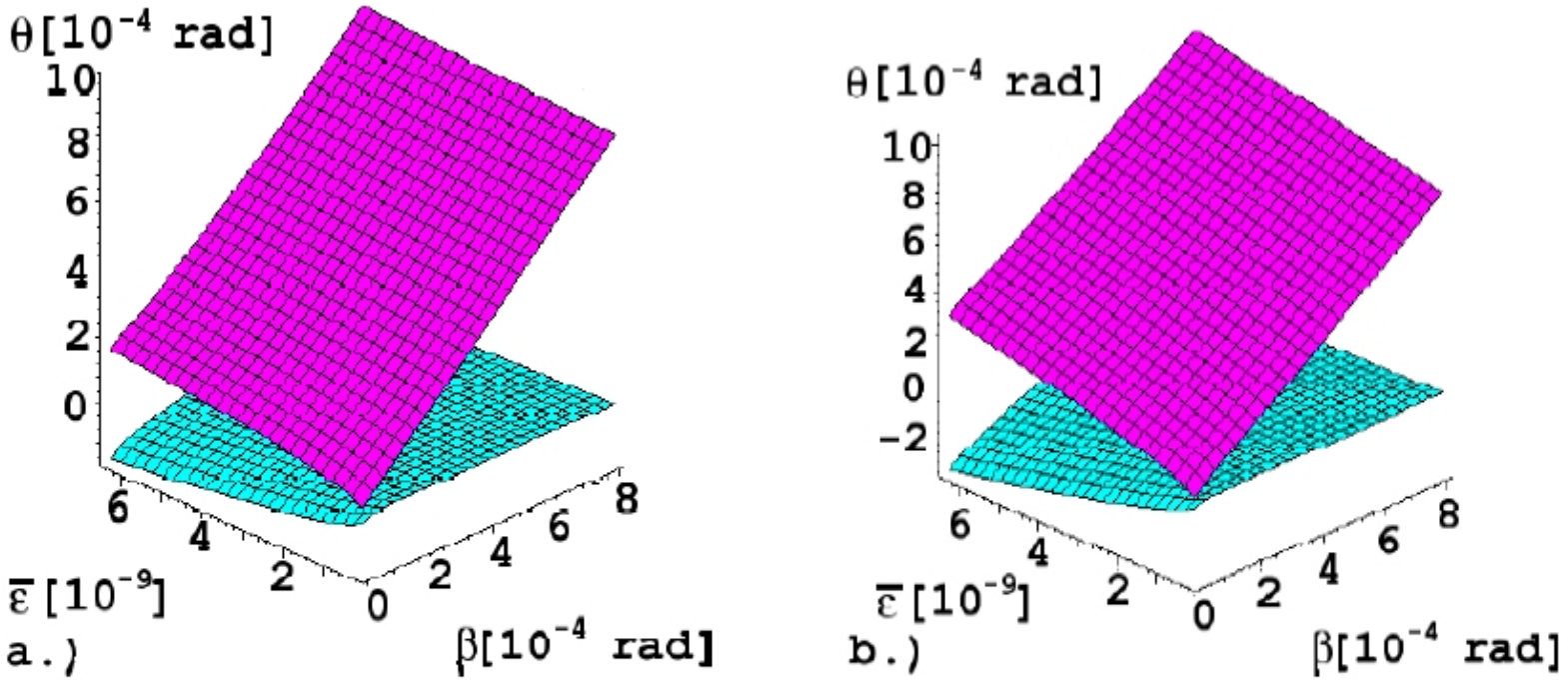

FIG. 3: The image positions θ as function of $\bar{\varepsilon}$ and β for $\sigma = 0.25$ (left) and $\sigma = 0.75$ (right), for the distances $D_l = 1$ Mpc and $D_{ls} = 2$ Mpc. The angle β is varied up to 0.0015 rad, similarly as on Fig 4b of Ref. [29]. With decreasing β, the images shrink accordingly. At $\beta = 0$ the angle θ represents the angular radius of the Einstein ring. As we expect the $\beta = 0$ sections of the surfaces are symmetric with respect to the plane $\theta = 0$.

- magnifications

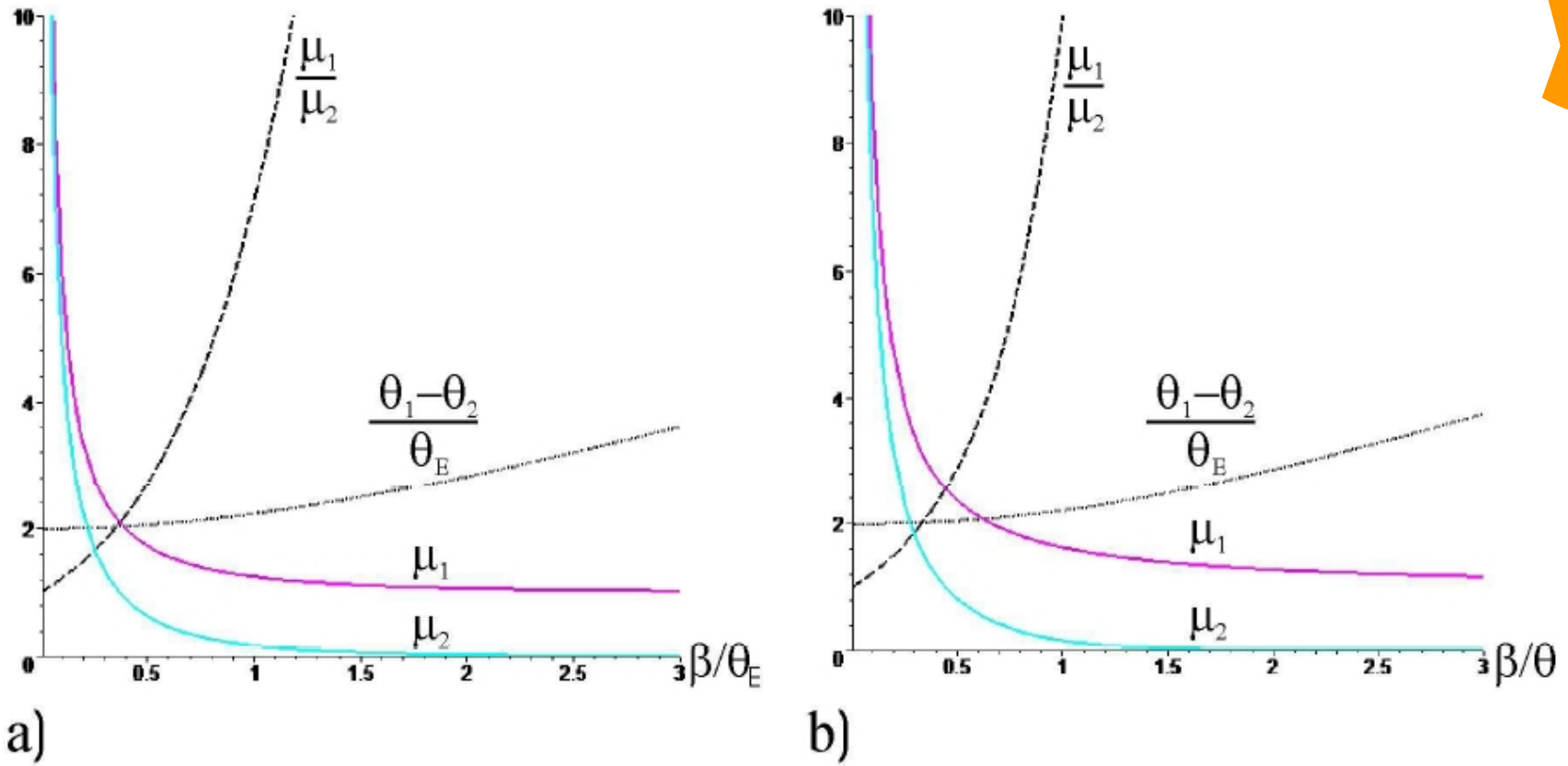

FIG. 4: The image separations and magnifications as functions of β/θ_E for $\sigma = 0.25$ (left) and $\sigma = 0.75$ (right). We fixed $\bar{\varepsilon} = 3.375 \times 10^{-9}$, while the distances $D_l = 1$ Mpc and $D_{ls} = 2$ Mpc were chosen for the plots. The upper and lower solid curves represent the primary and secondary image magnification factors, respectively; their ratio is the dashed curve; and the dotted curve is the normalized image separation.

- observable signature: the ratio of magnifications (flux ratio) has different power-law dependence on the image separations

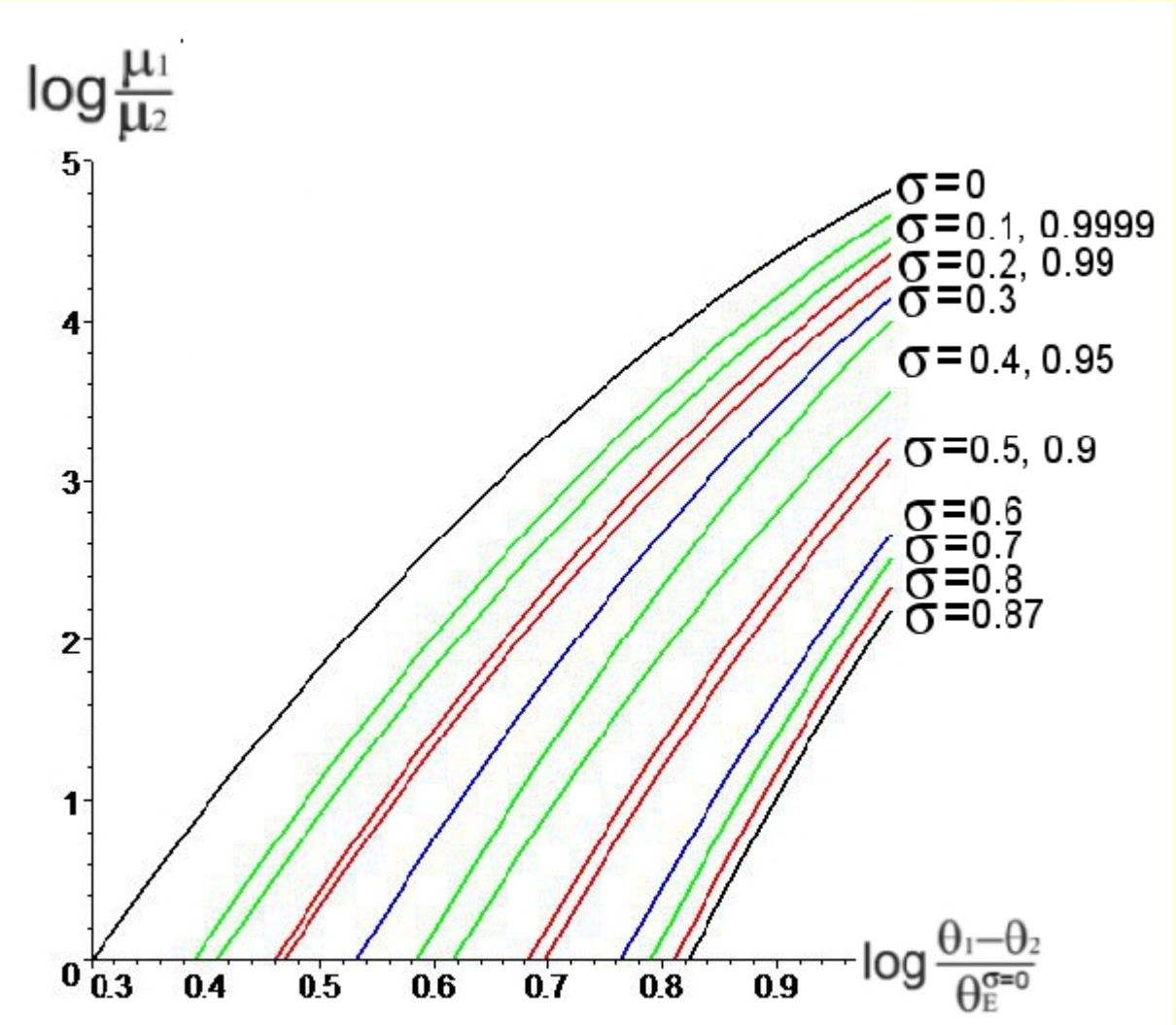

Weak gravitational lensing by fourth order gravity black holes

σ	0	0.1	0.2	0.3	0.4	0.5	0.6	0.7	0.8	0.87	0.9	0.95	0.99	0.9999
κ	4.39	4.87	5.21	5.64	6.15	6.69	7.20	7.60	7.84	7.92	6.60	5.92	5.12	4.87

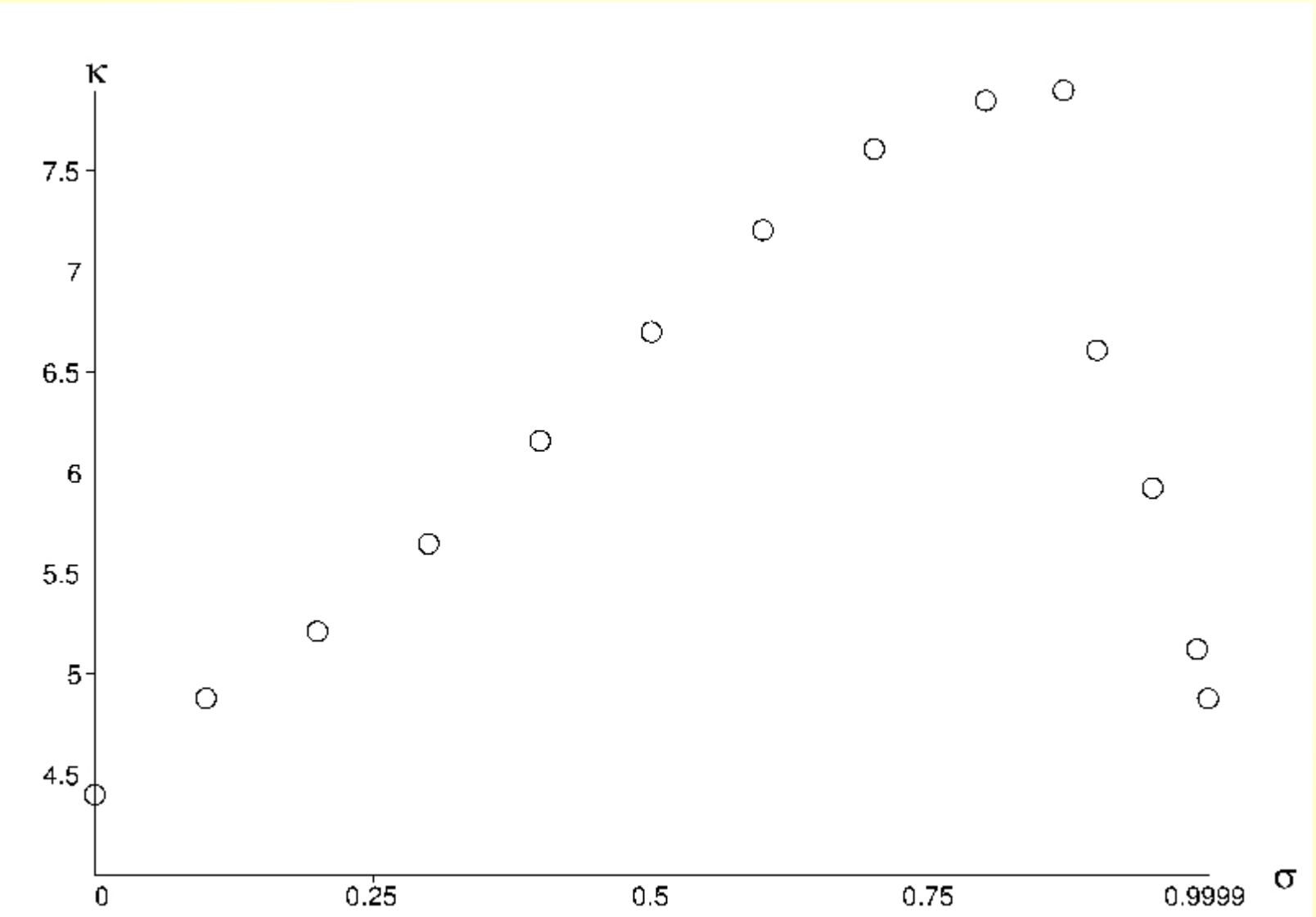

next generation of radio telescopes will do

Summary

- all alternative gravity theories imply
  an additional length scale
- gravitational lensing in principle could
  distinguish among these theories and GR
  and falsify some of them!
- critical phenomena, different power-law behaviour
- instrument resolution too low for now,
  may be sufficient in a few years

- non-trivial generalization: the rotating case